JGR Atmospheres

RESEARCH ARTICLE
10.1029/2025JD045176

Twenty-One Years of Global Atmospheric Chlorine Inventories From Atmospheric Chemistry Experiment Fourier Transform Spectrometer (ACE-FTS) Measurements

N. Raymond[1], P. Bernath[1,2], C. Boone[1], and M. P. Chipperfield[3,4]

[1]Department of Chemistry, University of Waterloo, Waterloo, ON, Canada, [2]Department of Chemistry and Biochemistry, Old Dominion University, Norfolk, VA, USA, [3]School of Earth and Environment, University of Leeds, Leeds, UK, [4]National Centre for Earth Observation, University of Leeds, Leeds, UK

Key Points:

- A detailed inventory of atmospheric chlorine from 2004 to 2024 was constructed using ACE-FTS measurements
- Total atmospheric chlorine volume mixing ratios showed an average trend of −9.56 ± 0.28 ppt per year
- Reduction of total atmospheric chlorine has been partially mitigated in recent years by the increasing contributions from Cl-VSLS

Supporting Information:

Supporting Information may be found in the online version of this article.

Correspondence to:

N. Raymond,
neil.raymond@uwaterloo.ca

Citation:

Raymond, N., Bernath, P., Boone, C., & Chipperfield, M. P. (2026). Twenty-one years of global atmospheric chlorine inventories from atmospheric chemistry experiment Fourier transform spectrometer (ACE-FTS) measurements. *Journal of Geophysical Research: Atmospheres*, *131*, e2025JD045176. https://doi.org/10.1029/2025JD045176

Received 16 AUG 2025
Accepted 18 JAN 2026
Corrected 28 MAR 2026

This article was corrected on 28 MAR 2026. See the end of the full text for details.

Author Contributions:

Data curation: M. P. Chipperfield
Funding acquisition: P. Bernath
Supervision: P. Bernath
Writing – review & editing: P. Bernath, C. Boone, M. P. Chipperfield

Abstract We present atmospheric chlorine inventories over 21 years (2004–2024) and five latitude bands (82–60°N, 60–30°N, 30°N–30°S, 30–60°S, 60–82°S) across altitudes from the surface up to 61 km. These inventories were calculated using the Atmospheric Chemistry Experiment-Fourier Transform Spectrometer (ACE-FTS) version 5.3 retrievals of the volume mixing ratios (VMRs) of 13 chlorine-containing species. Of these, five are product gases: HCl, HOCl, $ClONO_2$, COClF, $COCl_2$, and eight are source gases: CCl_4, CH_3Cl, CFC-11 (CCl_3F), CFC-12 (CCl_2F_2), CFC-113 ($CClF_2CCl_2F$), HCFC-22 (CHF_2Cl), HCFC-141b ($C_2H_3Cl_2F$), and HCFC-142b ($C_2H_3ClF_2$). Where necessary, ACE-FTS data were supplemented with data from the TOMCAT 3-D chemical transport model, the Aura Microwave Limb Sounder (MLS) instrument, and ground-based measurements from the National Oceanic and Atmospheric Administration (NOAA) and the Advanced Global Atmospheric Gases Experiment (AGAGE). Total chlorine (Cl_{tot}) profiles are dominated by source gas contributions in the troposphere and lower stratosphere. At lower altitudes, the primary contributors are chlorofluorocarbons (CFCs), chlorocarbons, and, increasingly in recent years, chlorine-containing very short-lived substances (Cl-VSLS). At higher altitudes, HCl becomes the dominant contributor comprising up to 99% of Cl_{tot} by 61 km. The relative contribution of individual species to Cl_{tot} showed that Cl-VSLS and HCFC-22 have partially slowed the reduction in atmospheric chlorine achieved by the phase-out of CFC production and consumption. Between 2004 and 2024, the global mean Cl_{tot} time series decreased by 9.56 ± 0.28 ppt/year (0.28 ± 0.01%/year), with values approaching 3.3 ppb in 2024. These findings demonstrate the significant impact of the Montreal Protocol in reducing emissions of substances that are both ozone-depleting and greenhouse gases.

Plain Language Summary Understanding the behavior, distribution, and climate impact of chlorine-containing molecules is important in an environmental context, in particular because of their strong ozone depletion potential. We estimated the total amount of chlorine from the surface up to 61 km, primarily using data from the Atmospheric Chemistry Experiment (ACE), a satellite-based mission that has been operational since 2004. We observed a decline in total chlorine over the past 21 years; however, increasing amounts of very short-lived species (Cl-VSLS) have partially mitigated this decline in recent years. If Cl-VSLS contributions to atmospheric chlorine continue to increase they may pose a challenge to ozone recovery efforts.

1. Introduction

The ozone layer is a vital component in protecting life on Earth from harmful ultraviolet (UV) radiation (Salawitch et al., 2022). Chlorine is a primary driver of stratosphere ozone depletion, acting as a highly efficient catalyst accelerating the breakdown of ozone molecules. When chlorine-containing compounds (formerly used in refrigeration, aerosol products, and other applications) ascend into the stratosphere, they are broken apart by UV light, releasing free chlorine atoms (Molina, 1996). A single chlorine atom can initiate a series of catalytic reactions that can destroy thousands of ozone molecules before it becomes deactivated (Fahey & Hegglin, 2011, Q. 15, p. 21). This process significantly thins the protective ozone shield, which absorbs harmful UV radiation (Lary, 1997). Understanding the sources of chlorine and its role in ozone depletion is essential to addressing environmental risks posed by these chemicals and the global efforts required to mitigate their impact.

The Montreal Protocol on Substances that Deplete the Ozone Layer, first signed in 1987 and now universally ratified, is one of the world's most successful environmental treaties. It has been a resounding success in reducing

the use of chlorine-containing ozone-depletion substances such as chlorofluorocarbons (CFCs), which were once widely used in refrigeration, foam blowing agents, solvents, and aerosol propellants (Molina & Rowland, 1974; WMO, 2018). Satellite and ground-based observations confirm that stratospheric chlorine levels are declining (WMO, 2022), a key trend for the stabilization and gradual recovery of the ozone layer. This reduction helps restore the natural ozone shield that protects life on Earth from harmful UV radiation as well as mitigating the associated health and ecological risks (McKenzie et al., 2019). Because chlorine-containing species affect both stratospheric ozone and the radiative budget, changes in their atmospheric abundance have implications not only for UV exposure but also for climate (UNEP, 2024). The success of the Montreal Protocol is a powerful example of international collaboration addressing global environmental threats. Continued assessment of ozone depletion requires accurate measurements of tropospheric "source" gases, stratospheric total chlorine and their evolution over time.

With much of atmospheric chlorine originating from anthropogenic emissions (Von Clarmann, 2013), measurements of total chlorine (Cl_{tot}) offer a dramatic reminder of the impact of human activity on the atmosphere. Networks of ground-based monitoring stations, such as those operated by the National Oceanic and Atmospheric Administration (NOAA) (NOAA, 2025) and the Advanced Global Atmospheric Gases Experiment (AGAGE) (AGAGE, 2025), provide routine atmospheric measurements of chlorine-containing "source gases" near Earth's surface. As these source gases are transported upward through the atmosphere, a combination of photochemical destruction and chemistry transfer chlorine atoms to other molecules including HCl, $ClONO_2$, ClO, and HOCl (Von Clarmann, 2013). In the stratosphere HCl and $ClONO_2$ are the primary chlorine reservoirs, and their total column abundance can be used as a proxy for total inorganic chlorine. Above 50 km, nearly all chlorine is found in HCl, a product gas (Zander et al., 1992). Space-based measurements of HCl at 50 km and above can be used to generate a lower bound of atmospheric chlorine inventory and could provide independent verification for Cl_{tot} derived from ground-based inventories (with an appropriate time-lag applied). Because HCFCs contribute a non-negligible amount of chlorine at these altitudes (Chirkov et al., 2016), estimating Cl_{tot} exclusively from HCl would yield a low bias. Space-based instruments measuring with broad spectral coverage in the infrared also generally measure the most prominent chlorine-containing source gases (CFCs, hydrochlorofluorocarbons (HCFCs), CH_3Cl), opening the possibility of viewing the altitude dependence of chlorine atoms transferred from source gases into reservoir species such as HCl, $ClONO_2$, and HOCl which is valuable information for developing and testing models that incorporate chlorine-containing species. Previous studies have observed altitude dependent chlorine inventories using data from the atmospheric trace molecule spectroscopy (ATMOS) mission flown on the Space Shuttle (Zander et al., 1992), from the Jet Propulsion Laboratory (JPL) MkIV balloon-borne Fourier transform spectrometer (FTS; Webster et al., 1994), and from the Atmospheric Chemistry Experiment Fourier transform spectrometer (ACE-FTS) in 2006 (Nassar et al., 2006) and 2013 (Brown et al., 2013). The 2006 work used 14 chlorine-containing species from the v2.2 data set and the 2013 work used 9 chlorine-containing species from the v3.0 data set. The current work employs ACE-FTS retrievals of 13 chlorine-containing species (ClO was excluded due to high variance) from the v5.3 data set.

This work uses ACE-FTS measurements, supplemented with NOAA, AGAGE, Aura MLS, and model data, to construct a vertically resolved chlorine inventory. Similar to our previous study of fluorine inventories (Raymond et al., 2025) we supplement ACE-FTS measurements of some species in the upper stratosphere (>30 km), using data from the TOMCAT 3-D chemical transport model (CTM; M. Chipperfield, 1999). We also incorporate ground-based measurements from NOAA & AGAGE. These include molecules not measured by ACE-FTS such as CFC-13, as well as molecules measured by ACE-FTS, to allow us to extend the inventory below 5 km (the lowest altitude of ACE-FTS retrievals). Additionally, the average yearly volume mixing ratio of ClO was estimated using data obtained from the Aura Microwave Limb Sounder (MLS) instrument, which provides consistent and well-characterized observations in the stratosphere (Waters et al., 2006). Inventories have been calculated using 26 chlorine-containing species (listed in Section 2) over five latitude bands between 82°S and 82°N for every year (2004–2024) of Atmospheric Chemistry Experiment (ACE)'s operation. The accuracy of ACE-FTS, number of species considered, and broad altitude coverage considered in this work enables a novel and high-quality reconstruction of the total atmospheric chlorine over the past two decades. This vertical coverage allows for detailed comparison of long term trends across the troposphere, stratosphere, and mesosphere.

In Section 2 we list the sources of data used in this work. We describe the calculation of the inventory and processing of data in Section 3. Results are discussed in Section 4, and our findings are summarized in Section 5.

2. Data

The Canadian-led satellite mission ACE (Bernath, 2017), launched by NASA in August 2003, continues to operate with minimal performance degradation. Its primary instrument is a high-resolution Fourier transform spectrometer that operates in the 750–4,400cm^{-1} (2.2–13.3 μm) spectral region. The ACE-FTS utilizes the Sun as a light source and measures atmospheric transmittance spectra, during sunrise and sunset, using the limb geometry (solar occultation).

The current version 5.3 of the ACE-FTS retrieval includes profiles of over 46 gaseous molecules, retrieved as described in (Boone et al., 2023). The ACE-FTS currently measures 14 chlorine-containing species, COClF, CFC-11 (CCl_3F), CFC-12 (CCl_2F_2), CFC-113 ($CClF_2CCl_2F$), HCFC-22 (CHF_2Cl), HCFC-141b ($C_2H_3Cl_2F$), HCFC-142b ($C_2H_3ClF_2$), $COCl_2$, CH_3Cl, $ClONO_2$, ClO, HCl, HOCl, and CCl_4. The retrieval limits of ACE-FTS species used in this work are shown in Table 1.

Ground based measurements from NOAA and AGAGE were used to supplement the ACE-FTS data. Measurements from NASA's Aura Microwave Limb Sounder (MLS) were used to estimate chlorine monoxide's (ClO) yearly VMR. Additionally, as many of the retrievals from ACE-FTS do not extend to the upper limit of this work (60 km), the TOMCAT 3D CTM is used to estimate contributions above the retrieval limits for selected molecules. The species used (and their source) are detailed in Table 1. With version 5.3 retrievals and 21 years of data (2004–2024) ACE-FTS is well positioned to provide a long term inventory of chlorine in the atmosphere.

The MLS on NASA's Aura satellite (Waters et al., 2006) provides geophysical profiles of atmospheric parameters, such as temperature and trace gases (including ozone, water vapor, and others), derived from individual satellite measurements. MLS measures atmospheric composition by observing thermal microwave emissions from the Earth's limb. Operating at multiple microwave and submillimeter wavelengths, MLS detects naturally occurring thermal radiation emitted by atmospheric gases. By scanning the limb across different altitudes, the instrument retrieves vertical profiles of temperature, pressure, and a variety of chemical species, including ozone, water vapor, and chlorine monoxide. MLS measurements have been used in a wide array of works: investigating ClO in the Antarctic (Connor et al., 2007; Nedoluha et al., 2016), as well as more recent work on ClO and HOCl trends (Froidevaux et al., 2021), and estimating the solar flux effects on ozone (Dhomse et al., 2022). The current work uses Aura MLS Level 2 data (version 5.0 (Livesey et al., 2022)) of chlorine monoxide's (ClO) volume-mixing ratio in place of ACE-FTS measurements. The large number of observations results in a reduced variance when assessing ClO, and consequently Cl_{tot}, over a broad scale: 2004–2024. This is particularly important given the strong diurnal behavior of ClO (Brune et al., 1990; Khosravi et al., 2013; Kreyling et al., 2013).

TOMCAT/SLIMCAT (hereafter TOMCAT) contains a detailed treatment of stratospheric gas-phase and heterogeneous chemistry including the major species in the O_x, NO_y, HO_x, Cl_y, and Br_y chemical families (M. Chipperfield, 1999; Feng et al., 2007). The model also has a comprehensive treatment of long-lived source gases including CH_4, N_2O, CFCs, HCFCs and HFCs, which are constrained by time-dependent surface mixing ratio boundary conditions. The model includes two brominated and four chlorinated very short-lived substances (VSLS). The model uses monthly mean fields of surface area density to constrain liquid H_2SO_4 aerosols and calculates the occurrence of liquid and solid polar stratospheric clouds (PSCs). For this study the model was run at a horizontal resolution of 2.8° × 2.8° with 32 hybrid sigma-pressure levels from the surface to ∼61 km. Horizontal winds and temperatures were specified from the European Center for Medium-Range Weather Forecast's (ECMWF) ERA5 atmospheric reanalyzes (Hersbach et al., 2020). Vertical motion is calculated from the divergence of the horizontal winds. The volume mixing ratio of source gases at the surface level were specified using data files compiled for WMO/UNEP (2022). These global mean surface volume mixing ratios define the long-term tropospheric source gas trends in the model. TOMCAT has been used in many previous studies looking at the distribution and trends of stratospheric gases. Recent examples include: ozone (Arosio et al., 2024; Dhomse et al., 2022), CFCs (S. A. Montzka et al., 2021), chlorinated species (Hossaini et al., 2019) and brominated species (Rotermund et al., 2021). For this study TOMCAT output was used to vertically extend ACE-FTS retrievals which are not available over the entire altitude range (0–61 km). Section 3 outlines how TOMCAT profiles were scaled to ACE-FTS retrievals at their upper end to capture the predicted chemical transport for each species.

Ground-based measurements from NOAA and AGAGE were used to supplement ACE-FTS data by extending the vertical profiles below 5 km (the lowest altitude of ACE-FTS retrievals), and including molecules not measured by ACE-FTS. These measurements help give a fuller picture of source emissions of chlorine-containing species.

Table 1
The Six Product (Cl_p) and 19 Source (Cl_s) Chlorine-Containing Species, Their Corresponding Data Sources, and the Altitude Ranges of ACE-FTS Retrievals

		Source			Altitude (km)	
Name	Formula	Surface	Satellite	Adj.	Polar	Equatorial
Product Species						
Hydrogen chloride	HCl		ACE	e	6–61	7–61
Hypochlorous acid	HOCl		ACE	e,p	13–40	17–40
Phosgene	$COCl_2$		ACE	e,p	8–24	11–29
Fluorophosgene	COClF		ACE	e,p	13–27	14–32
Chlorine nitrate	$ClONO_2$		ACE	e,t	10–41	10–36
Chlorine monoxide	ClO		MLS		20–50	20–50
CFCs						
CFC-11	CCl_3F	NOAA	ACE	g,t	5–25	5–28
CFC-12	CCl_2F_2	NOAA	ACE	g,t	5–31	5–35
CFC-113	$C_2Cl_3F_3$	NOAA	ACE	g,t	5–25	5–25
CFC-13	$CClF_3$	AGAGE		s		
CFC-114/CFC-114a	$C_2Cl_2F_4$	AGAGE		s		
CFC-115	C_2ClF_5	AGAGE		s		
HCFCs						
HCFC-22	$CHClF_2$	NOAA	ACE	g,t	5–25	5–25
HCFC-141b	$C_2H_3Cl_2F$	NOAA	ACE	g,t	6–21	6–21
HCFC-142b	$C_2H_3ClF_2$	NOAA	ACE	g,t	6–21	6–21
HCFC-124	C_2HClF_4	AGAGE		s		
HCFC-132b	$C_2H_2Cl_2F_2$	AGAGE		s		
HCFC-133a	$C_2H_2ClF_3$	AGAGE		s		
Halons						
H-1211	$CBrClF_2$	NOAA		g,t		
Chlorocarbons						
Carbon tetrachloride	CCl_4	NOAA	ACE	g,t	6–25	8–30
Chloromethane	CH_3Cl	NOAA	ACE	g,t	9–40	12–40
Methyl chloroform	CH_3CCl_3	NOAA		g,t		
Cl-VSLS						
PCE (Tetrachloroethene)	C_2Cl_4	NOAA		t		
Dichloromethane	CH_2Cl_2	NOAA		t		
Chloroform	$CHCl_3$	AGAGE		t		
1,2-dichloroethane	$C_2H_4Cl_2$		TOMCAT			

Note. The Adj. (profile adjustment) column identifies species whose vertical profiles were modified, with a full discussion provided in Section 3. The five ACE-FTS product species were extrapolated to 0 VMR at 4 km below their lowest retrieval, denoted by "e," and the eight ACE-FTS source species' profiles were extended below their lowest retrieval by interpolation to the ground-based measurement, as denoted by "g." Species whose ACE-FTS retrievals were vertically extended up to 61 km using a priori profiles are denoted by "p." Profiles for six species not retrieved by ACE-FTS were obtained by matching to a source profile as listed in Table S2 of Supporting Information S1, denoted by "s." Species whose profiles were vertically extended up to 61 km using TOMCAT data, are denoted by "t." A cutoff around 2 ppt was used when considering species not measured by ACE-FTS.

NOAA data (Dutton, Hall, Dlugokencky, et al., 2023; Dutton, Hall, Montzka, et al., 2023a, 2023b, 2023c, 2023d; Dutton & Hall, 2023; S. Montzka et al., 1993, 1994) were obtained from their global monitoring laboratory (GML), publicly available online: https://gml.noaa.gov/dv/data/. AGAGE data (Prinn et al., 2018; Prinn, Weiss, Arduini, Arnold, et al., 2024; Simmonds et al., 2017; Vollmer et al., 2017, 2021; Western et al., 2024) were obtained from: https://www-air.larc.nasa.gov/missions/agage/data/. Both NOAA and AGAGE have been measuring halocarbon abundances throughout the global atmosphere continuously since 1978. While AGAGE employs a network of high-precision instruments located around the world, enabling continuous measurements of a wide range of trace gases, NOAA uses both flask-based collection and high-precision on-site instrumentation analysis methods to achieve this same end. These measurement networks place an emphasis on long-lived species, such as CFCs and HCFCs, which have significant implications for climate change and ozone layer depletion. The distribution of stations is different for the two networks, but both networks provide global coverage at a variety of latitudes.

Although ACE measurements are taken globally, ground-based measurement stations used for supplementary data are predominantly located in the Northern Hemisphere. When possible, ground-based information was taken from stations in the same latitude band. Additionally, corrections for water vapor (NOAA and AGAGE report dry air mole fractions for surface measurements) are negligible compared to statistical and systematic errors reported for ACE data.

We included four chlorine-containing very short-lived substances (Cl-VSLS): CH_2Cl_2 (dichloromethane), $CHCl_3$ (chloroform), C_2Cl_4 (tetrachloroethene), and 1,2-dichloroethane (CH_2ClCH_2Cl, 1,2-DCA) for which we were able to source data. These species are among the most significant Cl-VSLS in terms of both emissions and contributions to stratospheric chlorine (Bednarz et al., 2022; Hossaini et al., 2019, 2024). In particular, their growth, and potential for growth, warrants ongoing close monitoring (Smith et al., 2024). Other Cl-VSLS species such as CH_3ClBr, CH_3ClI, C_2H_5Cl, C_3H_7Cl, 1,1-dichloroethane (CH_3CHCl_2), C_2Cl_6, C_2HCl_3 (TCE), and C_2HCl_6 (HCB) were not included in our analysis primarily due to a lack of readily available measurements, in part from limited observational coverage or low atmospheric concentrations.

3. Methodology

The globe was partitioned into five latitude bands: (82–60°N, 60–30°N, 30°N–30°S, 30–60°S, and 60–82°S). Data from ACE, MLS, NOAA, AGAGE and TOMCAT were used to compute product chlorine (Cl_p), source chlorine (Cl_s), and total chlorine (Cl_{tot}) for each year (2004–2024) and latitude band. The number of occultations used in each year and band are shown in Table S1 of Supporting Information S1. The descent of air within the polar vortex is a well established phenomenon (Kawamoto & Shiotani, 2000). To avoid measurements within the polar vortex distorting the overall averages, occultations from January to April within 82–60°N and from July to October within 60–82°S were removed from every year. Similar to our previous work on fluorine (Raymond et al., 2025) we use the term "source chlorine" (Cl_s) to represent the contribution to atmospheric chlorine from all species which are emitted from the surface and "product chlorine" (Cl_p) to represent the contribution to atmospheric chlorine from all species that result from their (Cl_s) decomposition.

The gradual conversion of emitted source gases into secondary product gases is visually apparent (see Figure 1) as the dominance of Cl_s from the surface to the troposphere, a balance between Cl_s and Cl_p in the lower stratosphere and dominance of Cl_p in the middle to upper stratosphere.

For a given year and latitude band the processing of each chlorine-containing species yields vertical profiles of volume mixing ratios (VMRs) for all available occultations on the ACE-FTS pressure grid, defined at 1 km intervals between the surface and 61 km. The 61 km limit reflects the upper extent of reliable HCl retrievals, the reservoir for almost all chlorine above 50 km. The resulting set of profiles is then used to compute Cl_p and Cl_s as the sum over their respective contributions (see Table 1)

$$\begin{aligned} Cl_p &= \sum_i n_i [S_i] = [HCl] + 2[COCl_2] + [COClF] + \cdots \\ Cl_s &= \sum_i n_i [S_i] = 3[CCl_3F] + 2[CCl_2F_2] + [CClF_3] + \cdots \end{aligned} \quad (1)$$

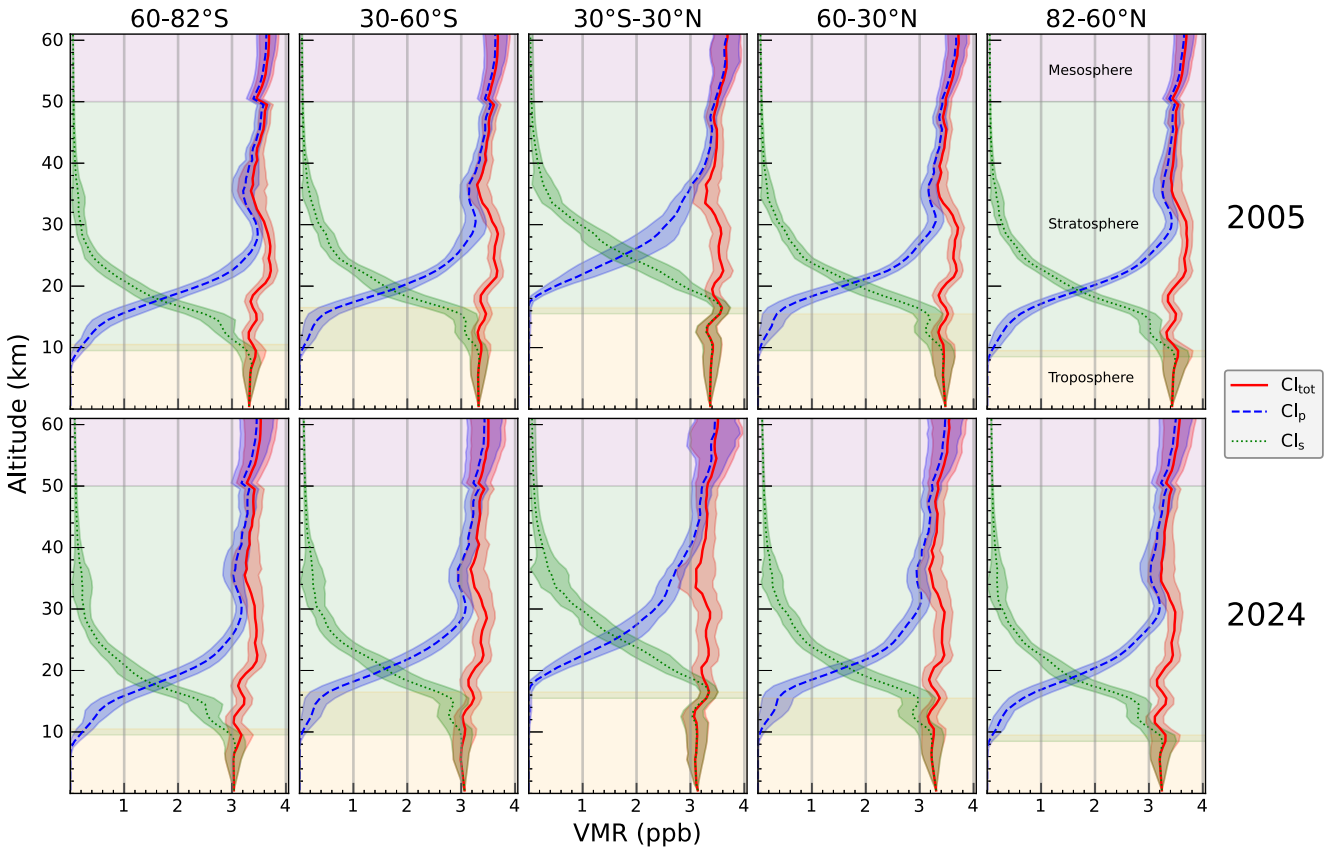

Figure 1. Mean total chlorine Cl_{tot} (red, solid), product chlorine Cl_p (blue, dashed) and source chlorine Cl_s (green, dotted) VMR profiles for 2005 (upper panels) and 2024 (lower panels) for each of the five latitude bands, within 0–61 km. Vertical gray lines, at 1, 2, and 3 ppb, are provided as a visual aid. Upper stratospheric differences in Cl_{tot}, Cl_p, Cl_s are more readily apparent when using these visual aids. All figures have identical *x* and *y* axes. Uncertainty (1σ) is represented by shaded envelopes.

where the prefactor n_i is the number of chlorine atoms in the species S_i. The total chlorine is computed as simply $Cl_{tot} = Cl_p + Cl_s$, which is equivalent to the total contribution from every species considered in this work. Following this, a 2.5 MAD (median absolute deviation) filter is applied to remove outliers from each of Cl_p, Cl_s, and Cl_{tot}. Finally, a single value, at each altitude, is computed as the mean over the remaining occultations. A more explicit outline of data processing is provided in Text S1 of Supporting Information S1. Uncertainties in the results section are purely random, represented by one standard deviation of the mean over the remaining occultations, with no systematic component. In this work, we refer to $n_i \times VMR_i$ as the "effective" VMR, which is useful for quantifying the relative influence of species (e.g., HCFC-22 and CFC-11) with similar VMR values (since $\sim$ 2010) but different numbers of chlorine atoms (1 vs. 3).

For species where ACE-FTS retrievals were not available a profile is constructed by taking a "source profile" and scaling it using a ground-based measurement of the species VMR. The species and their source profiles are listed in Table S2 of Supporting Information S1. HCFC-22 was used as a source for HCFC-124, HCFC-132b, and HCFC-133a. Due to their longer lifetimes (>100 years) CFC-13, ΣCFC-114 (CFC-114 + CFC-114a) and CFC-115 were matched to CFC-12, the longest liftetime CFC retrieved by ACE-FTS (the three CFCs retrieved by ACE-FTS, CFC-11, CFC-12, and CFC-113, have lifetimes of 52, 102, and 93 years, respectively (WMO, 2022)). See Text S1 in Supporting Information S1 for further discussion on the choice of source profiles. Quantification of the associated uncertainty was limited to the upper-stratospheric region (above 35 km) above the ACE-FTS retrieval range of the source profiles. In this region, the VMR contribution from scaled profiles is less than 5 ppt, smaller than the uncertainty (1σ) of Cl_{tot} as shown in Figure S1 of Supporting Information S1.

For species where ACE-FTS retrievals were available, processing of the raw data generally followed three steps: (a) standard ACE-FTS processing (Boone et al., 2023), (b) extension below the retrieval range to the surface (0 km), (c) extension above the retrieval range to 61 km.

To extend the retrievals below their range, a simple linear interpolation was used to generate points between the ground-based measurement and the lowest ACE-FTS-retrieved measurement for each occultation. We did not account for the time lag between surface emissions (as measured by NOAA and AGAGE) and atmospheric measurements by ACE-FTS (as described in Section 2.1 of (Schmidt et al., 2024)) as the effect was not readily apparent in our results. Likely these effects were mitigated by the use of five latitude bands, rather than calculating global averages, and sourcing ground-based measurements from stations within their respective latitude band. In situ surface measurements were not available for the six product species (Cl_p), therefore occultations were extrapolated to 0 VMR at 4 km below their lowest retrieval (excluding ClO).

To extend the retrievals above their range, except in the case of HCl, $COCl_2$, COClF, and HOCl, we used TOMCAT data. The retrieval range of HCl already spans the full vertical range used in this work (0–61 km). The profiles of $COCl_2$, COClF, and HOCl were extended upwards by scaling the a priori profiles. Note that a priori profiles for these three molecules come from ATMOS observations and include an extrapolated region above the highest analyzed altitude, as described in (Zander et al., 1992). The VMRs of $COCl_2$ and COClF drop below 5 ppt near the upper end of their ACE-FTS retrievals (24–29 km and 27–32 km, respectively), and the a priori and TOMCAT profiles are largely identical in the altitude regions above the ACE-FTS retrievals, trending to 0 VMR. ACE-FTS and TOMCAT HOCl in the middle stratosphere (near 35 km) generally exhibit a bias, which could indicate an issue for the chlorine partitioning in the model near this altitude. Many species have appreciable VMR, near this altitude: HCl, HOCl, CH_3Cl $ClONO_2$, ClO, as well as contribution from CFCs and HCFCs. Because direct ACE-FTS measurements are used to determine HCl contributions to the chlorine budget above 50 km, using scaled TOMCAT profiles for HOCl at this altitude could risk introducing a systematic bias. Fourteen species (CFC-11, CFC-12, CFC-113, HCFC-22, HCFC-141b, HCFC-142b, H-1211, PCE (C_2Cl_4), CCl_4 (carbon tetrachloride), $CHCl_3$ (chloroform), CH_2Cl_2 (dichloromethane), CH_3Cl (chloromethane), CH_3CCl_3 (methyl chloroform)) were extended upwards by scaling TOMCAT data. For a given year and species, the VMRs calculated by TOMCAT were available in a four-dimensional array: `(12, 32, 64, 128)`, corresponding to 12 months, 32 vertical pressure levels, and a horizontal grid of 64 latitude points (88°N–88°S) and 128 longitude points (0–360°E), with a width of roughly 2.8°. For a given year, latitude band and species, we averaged over the months, longitudes and latitudes (within the specified band) to produce an "average-VMR" profile over 32 vertical points (pressures in hPa). Note that TOMCAT uses a hybrid sigma-pressure vertical grid (with pure pressure levels in the mid-upper stratosphere) so model data are not evenly spaced (in units of km). To compare with ACE-FTS measurements we interpolated the aforementioned TOMCAT values onto a 1 km grid, in the same fashion as previous work (Harrison et al., 2016; Raymond et al., 2025). A scaling factor γ was computed as the average ratio of ACE-FTS/TOMCAT at the five highest ACE-FTS retrievals layers. Above the highest retrieval level, TOMCAT VMRs were multiplied by γ and used to extend retrievals up to 61 km.

The effect of using TOMCAT, as opposed to other approaches, to determine the slope of HCFCs (and other species) in the stratosphere contributes <5% to the mean (vertical) Cl_{tot}. Text S1 in Supporting Information S1 outlines the estimation of these % contributions. The use of these profiles may introduce some bias to Cl_{tot}, but the effect is minimal in comparison to the primary sources of uncertainty, HCl, HOCl, and $ClONO_2$, in the middle and upper stratosphere. Species specific uncertainties (1σ) within 35–45 km are approximately 100's of ppt for HCl, 50's of ppt for HOCl and $ClONO_2$, 10's of ppt for CCl_4, CFC-11, CFC-12, and HCFC-22, 1–9 ppt for HCFC-142b, CFC-113, COClF and less than 1 ppt for other species (excluding ClO).

While the average vertical profile of ClO retrievals from ACE-FTS is consistent with the other species in this inventory, and in particular Cl_{tot}, the variance within a year is extremely large ($\sigma \approx$ 1–2 ppb). The strong diurnal variation of ClO is driven by photochemistry and can exhibit enhancements on the order of 0.1 ppbv. To address this problem we used Level 2 ClO data (version 5.0) from the Aura MLS to compute average yearly profiles. For a given year and latitude band the MLS data was first screened using the provided Pressure (147–1.0 hPa), Precision (>0), Status (== 0), Quality (>1.3), and Convergence (<1.05) filters as outlined in the version 5.0 Data Quality document (Livesey et al., 2022). Measurements during morning were selected by filtering for data points whose local solar time was in the morning ($LocalSolarTime < 5$), with data points being predominantly either 02 or 03 hr (local solar time). MLS ClO vertical profiles were available at 37 pressure levels within 147–1 hPa. After

applying the screening criteria and restricting the data set to morning measurements, the remaining MLS profiles for each year and latitude band were averaged to yield a single value at each MLS pressure level. Converting the pressure values from hPa to atm, the single averaged MLS vertical profile was interpolated onto the retrieved ACE-FTS pressure for each individual ACE-FTS occultation, as ACE-FTS occultations have unique pressure grids. We discarded interpolated values below 20 km (roughly 60 hPa), avoiding the negative bias, largest at 100 and 147 hPa, as described in the version 5.0 Data Quality document (Livesey et al., 2022). Note that the VMR of ClO, as measured by ACE-FTS or MLS, below 20 km is small (<1% of Cl_{tot}). Finally, we take the yearly average over all interpolated occultations, producing a fixed contribution at each altitude between 20 and 50 km, which is then applied to Cl_{tot} and Cl_p. Note that we exclude MLS measurements from the polar vortex just as we did for ACE-FTS measurements as described in Section 3. Additional detail on MLS data processing is provided in Text S1.4 of Supporting Information S1.

In our investigation we found that using an annually averaged morning MLS ClO profile, added as a fixed contribution to Cl_{tot} and Cl_p, resulted in the most consistent Cl_{tot} profile for each year and latitude band. A further discussion on the comparison of MLS and ACE-FTS ClO measurements is provided in Text S1 of Supporting Information S1.

4. Results and Discussion

4.1. Vertical Cl_{tot} Profiles

Mean VMR profiles of Cl_{tot}, Cl_p, Cl_s for each latitude band are shown in Figures S2–S6 of Supporting Information S1. These profiles are shown from 0 to 61 km for each year between 2004 and 2024. A condensed view is provided in Figure 1 which compares 2005 and 2024 for each latitude band. The troposphere, stratosphere, and mesosphere are qualitatively represented by background colors of orange, green, and purple, respectively. The shaded overlap indicates tropopause height variability by latitude, most evident in the mid-latitudes of both hemispheres. The uncertainty of Cl_{tot} is largely consistent year-to-year and across latitude bands, with the exception of high altitudes (above 50 km) in the tropics (30°N–30°S). The uncertainty of Cl_p is greatest between 20 and 35 km in this region. These uncertainties represent the spread of the filtered occultations, as described in the previous section.

In Figure 1 and Figures S2–S6 in Supporting Information S1, we can clearly see the decomposition of Cl_s species into Cl_p species occurring primarily in the lower stratosphere. The cross-over point (where Cl_s and Cl_p have equivalent contribution to Cl_{tot}) appears relatively consistent from 2004 to 2024: 19, 23, 31, 25, and 23 km for 82–60°N through 60–82°S, respectively.

Figure 2 highlights the changes in Cl_{tot} between 2005 and 2024 for each latitude band. Although Cl_{tot} varies by latitude, the decrease over 21 years (200–300 ppt) is apparent. The prevalence of emissions occurring in the Northern Hemisphere is readily apparent when comparing Cl_{tot} (red) profiles in the troposphere, which show a difference of roughly 0.1 ppb between 82–60°N and 60–82°S. In contrast, stratospheric Cl_{tot} VMRs are roughly similar within uncertainties, representative of the well-mixed air over the entire globe. In the middle stratosphere (20–30 km), differences between 2005 and 2024 appear fairly consistent across latitude bands. Curvature in certain regions (e.g., 16–20 km at 30°S–30°N) may indicate biases in species' profiles.

Figures 3 and 4 provide a more detailed breakdown of contributions to Cl_{tot}, Cl_p, and Cl_s in the 60–30°N and 30–60°S latitude bands. It is obvious that the curvature of Cl_s and Cl_{tot} between 10 and 18 km is primarily driven by CH_3Cl (methyl chloride). The curvature of Cl_s and Cl_{tot} is also influenced by Cl-VSLS, whose increasing inter-latitudinal variability leads to discernible differences between latitude bands in both quantities. A decrease in effective CFCs from 2005 to 2024 is also visible (2.1 → 1.85 ppb), though less pronounced. Results for all five latitude bands are provided in Figures S7–S11 of Supporting Information S1.

Two phenomena are present in the Cl_{tot} profiles: a S-shaped feature between 10 and 18 km and a local maximum near 20–30 km, which can be more readily seen in Figures S7–S11 of Supporting Information S1. We believe CH_3Cl is primarily responsible for the S-shaped feature, discussed further below. The 20–30 km local maximum appears strongly influenced by $ClONO_2$ and generally occurs just above the crossover point, where source and product gases are similar in magnitude (and where both are changing rapidly with altitude). These phenomena present differently in the Southern, Northern, and tropical latitude bands.

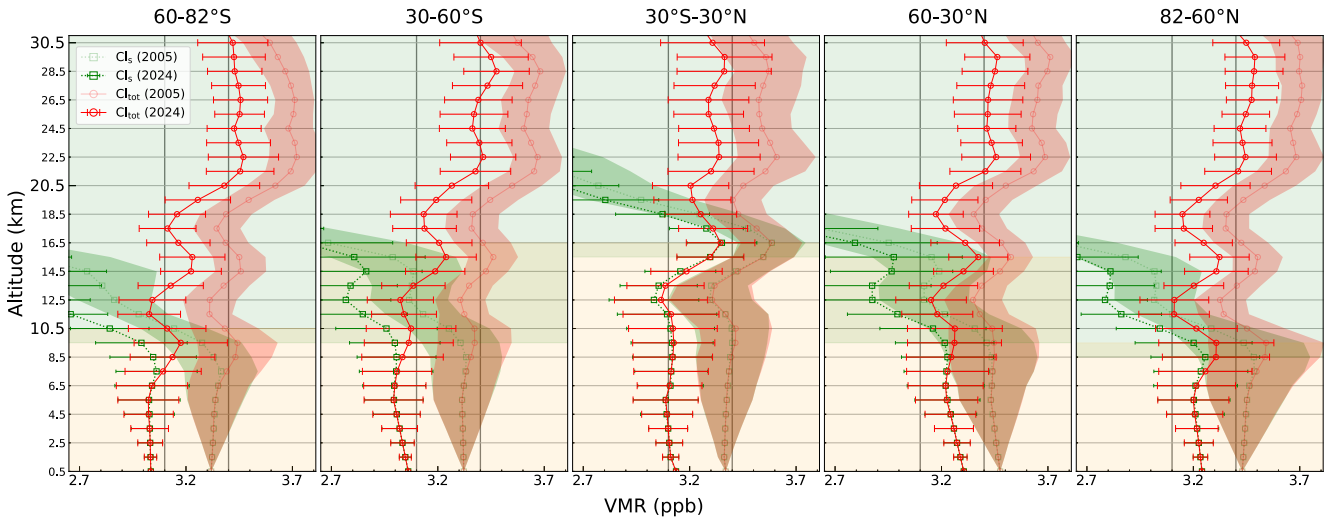

Figure 2. The mean total chlorine Cl_{tot} (red, circles, solid lines), and source chlorine Cl_s (green, squares, dotted lines) VMR profiles for 2005 and 2024 for each of the five latitude bands, within 0–30 km. Profiles for 2005 are shown as transparent (faded) curves, while those for 2024 are shown as opaque curves. Vertical gray lines at 3.1 and 3.4 ppb are provided as a visual aid. All panels have identical *x* and *y* axes. Uncertainty (1σ) is represented by shaded envelopes for 2005 and by error bars for 2024. Background altitude shading indicates the troposphere and stratosphere.

The vertical profile of CH_3Cl exhibits an anomalous S-shaped feature between 10 and 18 km, that is, latitudinally dependent. The profile presents as a high bias at 14–18 km and a low bias at 10–14 km, with a maximum deviation of approximately 0.2 ppbv across all five latitude bands. We discuss three possible factors that may, in some part, contribute to this shape: seasonal variation, latitudinal variation, and line-mixing effects. Ground-based measurements from AGAGE and NOAA show interhemispheric differences and seasonal variation. Prior work (Khalil & Rasmussen, 1999) estimated the seasonal variation of stratospheric and lower mesospheric CH_3Cl with maximal differences on the order of 0.1 ppbv. At this time, yearly averages of species are calculated without corrections for seasonal variations. The resulting vertical profiles are clearly latitudinally dependent. The vertical profile of 60–82°S is unique, showing a relatively uniform profile below 16 km, with the exception of a slight low bias between 10 and 13 km. The 30–60°S and 60–30°N bands have similar profiles. Qualitative figures are included in the supplementary material (Figures S12–S14 in Supporting Information S1) for illustrative purposes, but detailed analysis of the CH_3Cl profile, and its temporal and latitudinal variation are left to future studies. At this time ACE-FTS does not account for line-mixing effects (Bray et al., 2012; Ma & Boulet, 2021) in the retrieval of CH_3Cl, which could account for some part of the low bias near 10–13 km. One might also consider whether the exclusion of the polar vortex occultations (as previously described) is a contributing factor. However, the vertical profile for 82–60°N, which would have the corresponding northern occultations removed, does not appear to be consistent with this explanation. In contrast, the tropical band shows a high bias throughout 14–19 km, consistent with observations of elevated CH_3Cl emissions in tropical latitudes (Khalil & Rasmussen, 1999). However, the VMR in this altitude range is on the order of 0.2 ppbv higher than ground-based measurements. It would be unexpected that transport effects alone are responsible for these differences.

In our previous work (Raymond et al., 2025) we observed a "dip" in total atmospheric fluorine around 18 km, which we believed to be primarily associated with an inconsistency between the spectroscopic information for weak CO_2 lines used to derive pressure, temperature, and pointing information for ACE-FTS spectra above 18 km and the spectroscopic information for N_2 collision induced absorption that provides pointing information below 18 km (Boone et al., 2023). A similar "dip" in Cl_{tot} would be expected, given the use of ACE-FTS retrievals, however the intensity of the S-shaped feature of CH_3Cl largely obscures the phenomenon. Although a case could be made for the presence of the "dip" in the tropical band (Figure S4 in Supporting Information S1), the substantial changes to various species' VMR within that altitude range makes attribution to a single cause unclear.

The profiles of three chlorinated very short-lived substances (Cl-VSLS) included in this work (PCE (C_2Cl_4), chloroform ($CHCl_3$), and dichloromethane (CH_2Cl_2)) are ground-based measurements (NOAA/AGAGE) vertically extended by scaling TOMCAT profiles. The contribution of 1,2-dichloroethane (CH_2ClCH_2Cl, 1,2-DCA) is taken directly from TOMCAT model data due to a lack of available ground-based measurements

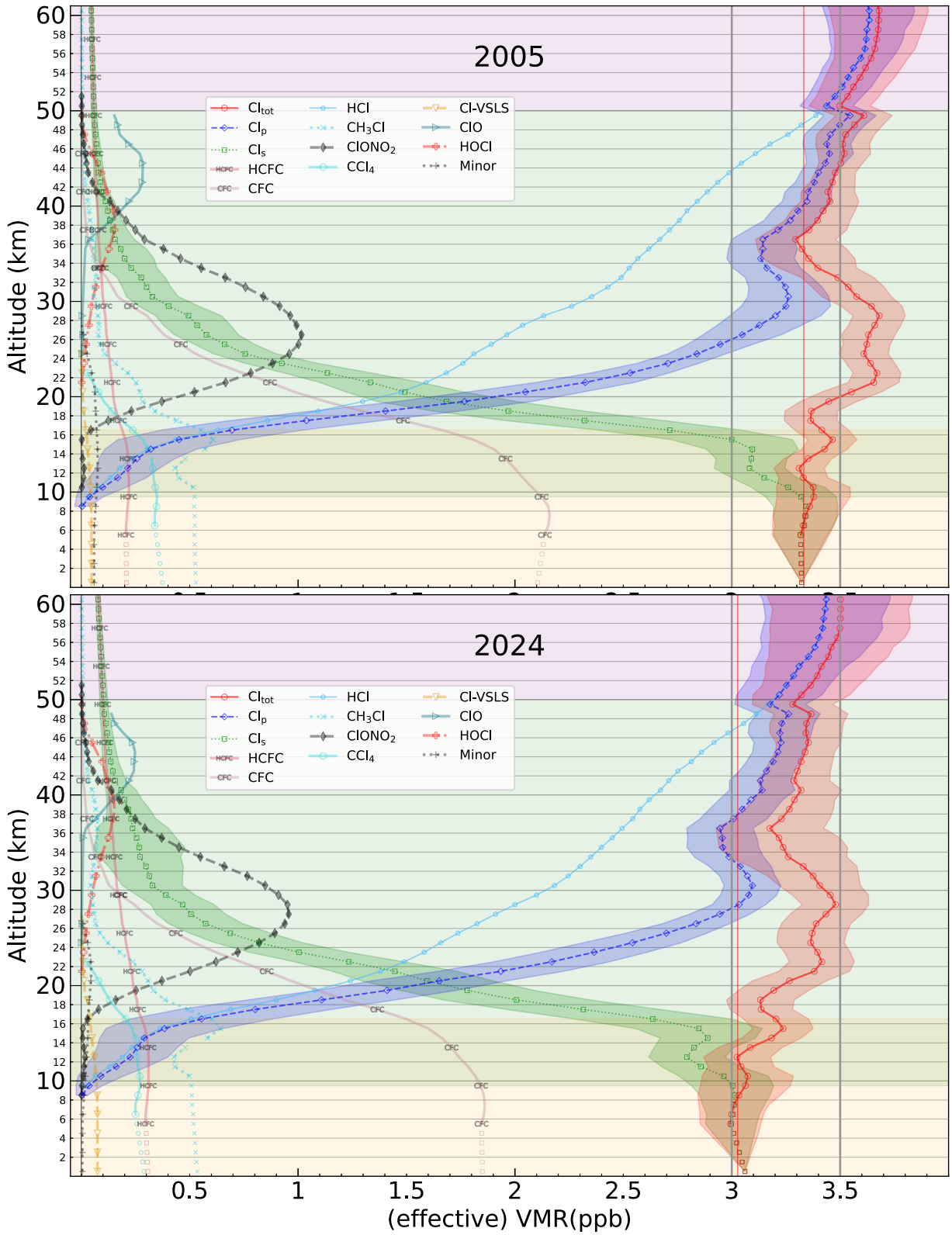

Figure 3.

(Hossaini et al., 2024). Comparing the 2024 Cl_{tot}, Cl_s, and Cl_p profiles in the 30–60°S and 60–30°N bands (Figures 3 and 4) reveals a roughly 200–300 ppt tropospheric difference. Above 20 km, where VSLS have largely decomposed and the air is well mixed, the profiles are largely similar between the hemispheres. Previous studies have also documented the contribution of Cl-VSLS to total atmospheric chlorine (Bednarz et al., 2022; Tegtmeier, 2019). Although Cl-VSLS estimates in this study are not derived from ACE-FTS, their inclusion is necessary to construct a complete atmospheric chlorine budget. As they decompose into product species, their contribution has measurable effects above the troposphere, influencing the concentrations of constituents retrieved by the ACE-FTS.

4.2. Assessing Inventory Completeness

A straightforward method for assessing if all necessary species were included is to correlate the source and product (sometimes referred to as reservoir) species. This analysis indicates imbalances between the source species, which decompose in the stratosphere, and the product species. We calculated the Pearson correlation coefficient r between Cl_s and Cl_p for each year and latitude band. These values are presented in Table S3 of Supporting Information S1. All coefficients were less than −0.99 demonstrating a strong inverse correlation between Cl_s and Cl_p. It is therefore reasonable to conclude that the major contributing chlorine-containing species have been included in this budget. This is consistent with Table 1-7 of the 2022 Ozone Assessment which lists HCFCs, CFCs, CCl_4, and CH_3Cl as contributing >95% of tropospheric Cl_{tot} (WMO, 2022, Chapter 1, p. 91). We note, however, the increasing role played by tropospheric Cl-VSLS in recent years, which highlights the need for careful observation in the context of tracking and measuring Cl_{tot} in the future (M. P. Chipperfield et al., 2020; Dubé et al., 2025; Hossaini et al., 2019).

4.3. Species Relative Contribution to Cl_{tot}

Figure 5 and Figures S15–S19 provide a qualitative representation of the change in individual species' relative (%) contributions to Cl_{tot} between 2005 and 2024 (similar to Figure 4 and Figures S7–S11 in Supporting Information S1). In the troposphere and lower stratosphere Cl_{tot} is dominated by CFC-11 and CFC-12, accounting for roughly 30%–55% of Cl_{tot}, while in the middle to upper stratosphere HCl eventually accounts for 99% of Cl_{tot}. The most apparent feature is how readily CFCs decompose, contributing in large part to $ClONO_2$ and HCl.

The dominant contributors to Cl_{tot}, HCl, CFC-11, and CFC-12, are compared in Tables 2 and 3 for the years 2005 and 2024. Altitude ranges were chosen based on a relative (%) contribution cut-off closest to 20% (absolute) allowing for improved latitude comparison as the height of the troposphere is not static across the latitude bands. Additionally, it more accurately captures the dynamic behavior of these species, evolving over time in both quantity and locality. For example, CFC-12 continues to account for nearly one-third of Cl_{tot} near the surface. Higher in the profile, the altitude at which its contribution reaches the 20% (of Cl_{tot}) cut-off is about 1 km lower in 2024, indicating a slower response of the upper-altitude burden. The lower altitude cutoff for HCl remains consistent, although changes in absolute VMR appear to show a latitudinal bias, with 30–60°S and 30°N–30°S declining by 90 ppt, compared to only 10–30 ppt in the remaining latitude bands. CFC-11's contribution at higher altitudes also appears to have a latitudinal bias. The cause is unclear; it may be chemical, photolytic, related to transport, or numerical in nature (e.g., due to the altitude space representation). The contribution from CFC-11 at higher altitudes declines more rapidly than CFC-12, as expected due to its shorter atmospheric lifetime. At the surface, the effective VMR of both CFC-11 and CFC-12 decreased by approximately 220 ppt between 2005 and 2024. At the highest altitude of this work (61 km) HCl's VMR declined by approximately 190 ppt. These changes speak to the success of the Montreal Protocol in reducing Cl_{tot}, which has a direct impact on the ozone layer, via controls on the production and consumption of long-lived chlorine containing substances.

Figure 3. Mean VMRs of Cl_{tot}, Cl_p, Cl_s and effective VMRs of chlorine-containing molecules for 2005 (upper panel) and 2024 (lower panel) in the latitude band 30–60° S, within 0–61 km. Cl_{tot}, Cl_p, Cl_s are shown using a solid line with circle markers, a dashed line with diamond markers, and a dotted line with square markers, respectively; their uncertainties (1σ) are represented by shaded envelopes. HCFCs, CFCs, Cl-VSLS, and Minor species (COClF, $COCl_2$, CH_3CCl_3, and H-1211), are grouped together to improve visual clarity. MLS ClO contributions are restricted to 20–50 km, as noted in the main text. Several species' markers are plotted every second altitude level to reduce crowding. A thin vertical red line indicates the mean value of Cl_{tot} from 0 to 10 km. Horizontal gray lines are spaced every 2 km to aid with visual identification of altitude. Values below 0.1 ppt are omitted to enhance clarity. Where plotted series appear only as discrete markers, the values represent interpolated points between the lowest ACE-FTS retrieval and ground-based measurements.

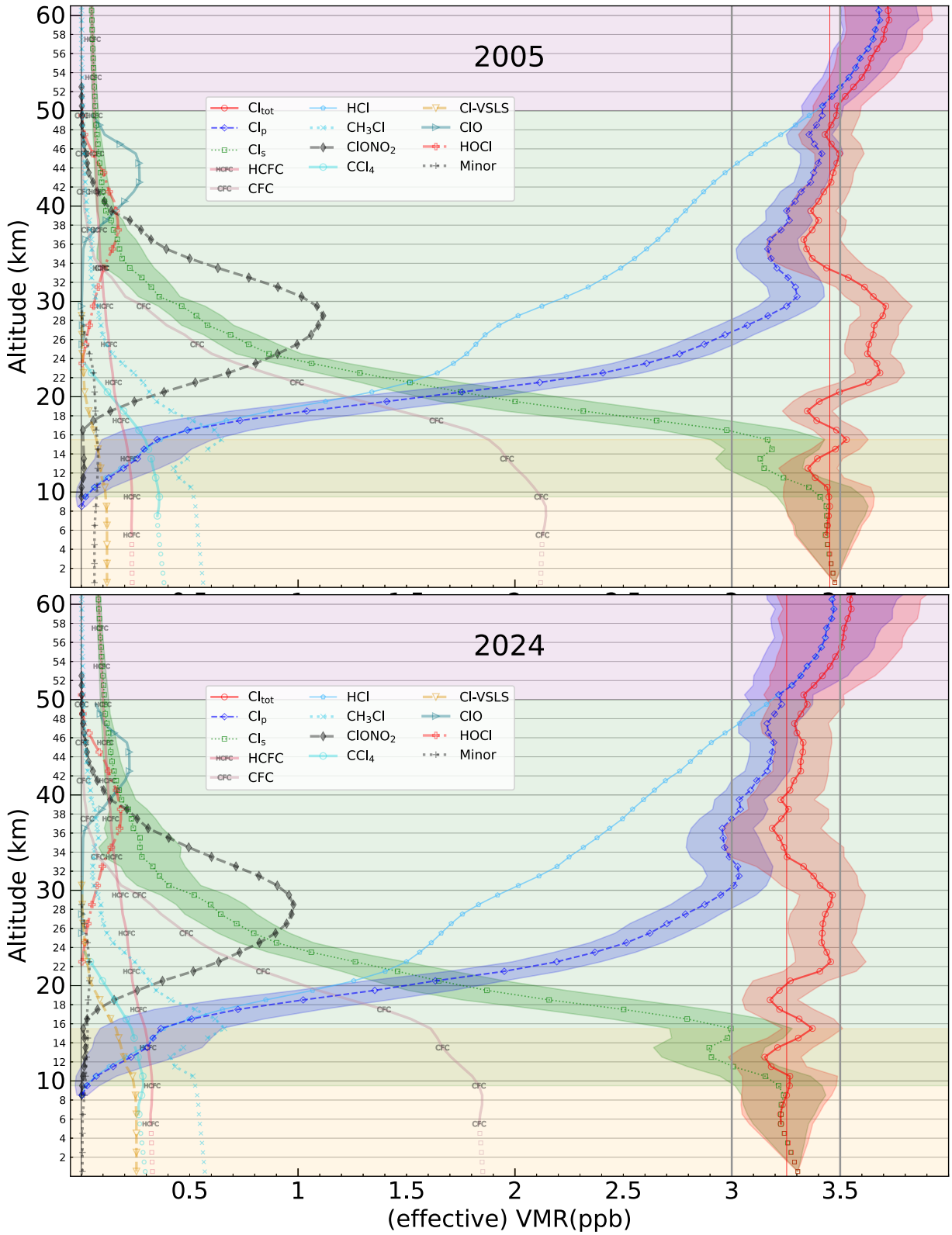

Figure 4.

To assess broad-scale changes in the relative contributions of source species over the 2004–2024 period, we computed weighted total column abundances (TCA) for four groups (HCFCs, CFCs, chlorocarbons, and Cl-VSLS) and compared them with the TCA of Cl_{tot}. The TCA for each species represents the vertically integrated product of their VMR and the ACE-FTS air density profile, yielding absolute abundances. Throughout this work TCAs are reported in molecules/cm^2. Each group's TCA was computed as the sum of the abundance of their constituent species, weighted by the number of chlorine atoms per molecule. This approach is a column-integrated metric and does not capture changes in vertical distribution, like those illustrated in Figures 4 and 5. To reduce the influence of group-specific outliers and temporal variability, an additional 2.5 MAD filter was applied to the occultations prior to computing the weighted TCAs. Figure 6 shows the evolution of each group's contributions in the 60–30°N latitude band, expressed relative to their minimum value within 2004–2024. This representation highlights the increase in the contribution from Cl-VSLS in recent years. The effect of the MAD filter is visible as a minor discrepancy between the top of the stacked areas and the TCA of Cl_{tot}. Agreement with the TCA of Cl_{tot} serves as a secondary validation that relative magnitudes have been preserved. As a quantitative summary, Table 4 presents the percent contribution and absolute VMR of Cl-VSLS in 2005 and 2024. Notably, the percent contribution more than doubled in the 60–30°N and 82–60°N bands. In contrast, Cl-VSLS VMRs remain substantially lower in the 30–60°S and 60–82°S bands, even in the stratosphere. As discussed in the following section, the increased contribution from Cl-VSLS has partially mitigated the decline in Cl_{tot} driven by reductions in CFCs and chlorocarbons.

4.4. Trend of Total Chlorine

The annual trends of Cl_{tot} between 2004 and 2024 are reported in Table 5 and plotted in Figure 7. The trend for each latitude band was computed as a least-squares fit to the average Cl_{tot} (0–61 km) over all years. Hemisphere and global trends were calculated by averaging the previously calculated trends from individual latitude bands. This was done to avoid biasing the trends as ACE-FTS has significantly more occultations near the poles than the equator (see Table S1 in Supporting Information S1). Systematic errors are not considered, as they are not calculated for ACE-FTS. We expect minimal effect from systematic errors as they will be consistent between years (ignoring potential systematic drifts in the retrieval results). Because all years were treated identically (identical altitudes, latitudes, filtering), fixed systematic errors are expected to cancel when computing yearly trends.

The estimated annual trend shows Cl_{tot} decreased globally by 9.56 ± 0.28 ppt/year, or 0.28%/year, over the 2004–2024 period. Most latitude bands show a similar rate of decline. However, we must again note that the number of ACE-FTS occultations in the tropical band is less than half at the poles (see Table S1 in Supporting Information S1). Stated roughly, ground-based measurements of Cl_{tot} in 60–30°N changed by 0.2 ppb from 2004 to 2024 (3.5 $\rightarrow$ 3.3 ppb), representing a decrease of 9.5 ppt/year over a 21 year period. Despite the Montreal Protocol's successful reduction of CFCs, CCl_4 and CH_3CCl_3 abundances, the rate of decrease of Cl_{tot} has been slowed down. This slowdown is partially due to increasing emissions of HCFCs and Cl-VSLS; evident in rising VMRs, increasing relative contribution to Cl_{tot}, and higher total column abundances, as previously shown in Figures 4–6, respectively.

To evaluate the global trend of total chlorine (Cl_{tot}), we compared our results with ground-based total chlorine measurements from NOAA and AGAGE. Our approach intentionally minimized data modification on the part of the authors, using NOAA and AGAGE records as reported, to prevent the introduction of bias. Good agreement would imply that the selection of ground-based observations within the latitude bins can be regarded as a reasonable approximation of the true zonal mean without significant bias. The global tropospheric total chlorine NOAA values included HCFC-22, HCFC-141b, HCFC-142b, CFC-11, CFC-12, CFC-113, CCl_4, and H-1211, with a constant offset of 0.7 ppb to account for CH_3Cl, CH_2Cl_2, and other trace gases (Data were obtained from (NOAA-data, 2025); with recent 2024 data generously provided by Stephen Montzka). AGAGE values were

Figure 4. Mean VMRs of Cl_{tot}, Cl_p, Cl_s and effective VMRs of chlorine-containing molecules for 2005 (upper panel) and 2024 (lower panel) in the latitude band 60–30° N, within 0–61 km. Cl_{tot}, Cl_p, Cl_s are shown using a solid line with circle markers, a dashed line with diamond markers, and a dotted line with square markers, respectively; their uncertainties (1σ) are represented by shaded envelopes. HCFCs, CFCs, Cl-VSLS, and Minor species (COClF, $COCl_2$, CH_3CCl_3, and H-1211), are grouped together to improve visual clarity. MLS ClO contributions are restricted to 20–50 km, as noted in the main text. Several species' markers are plotted every second altitude level to reduce crowding. A thin vertical red line indicates the mean value of Cl_{tot} from 0 to 10 km. Horizontal gray lines are spaced every 2 km to aid with visual identification of altitude. Values below 0.1 ppt are omitted to enhance clarity. Where plotted series appear only as discrete markers, the values represent interpolated points between the lowest ACE-FTS retrieval and ground-based measurements.

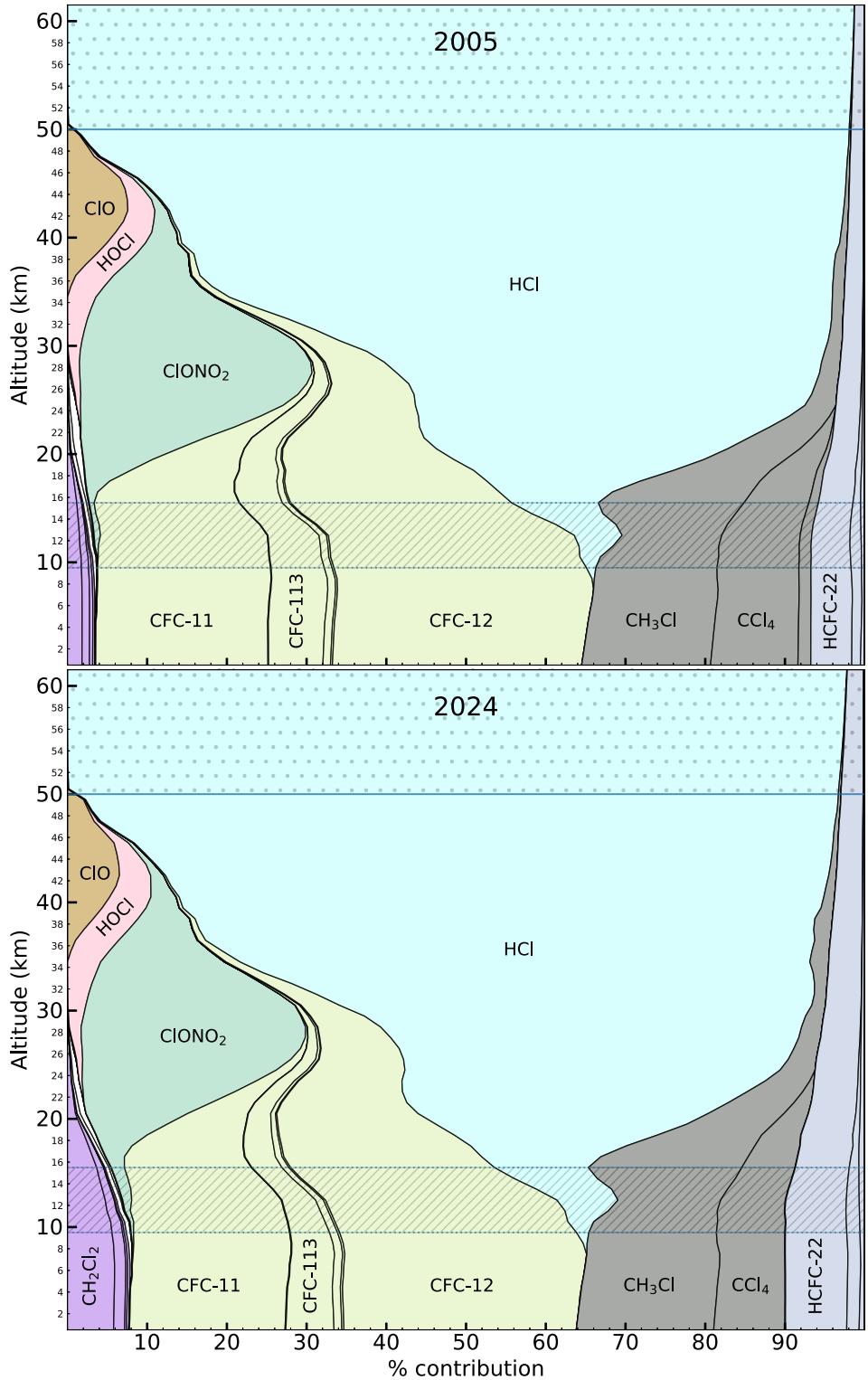

Figure 5. Percent contribution to Cl_{tot} of each chlorine-containing species for 2005 (upper panel) and 2024 (lower panel) in the latitude band 60–30°N, within 0–61 km. Common groups of species are colored similarly to improve visual clarity. HCFCs are steel-blue, CFCs are lime green, Chlorocarbons are gray, Cl-VSLS are lavender, and Minor species (COClF + Halons) are colored white (in-between Cl-VSLS and $ClONO_2$). A dashed region indicates the tropopause and a blue line indicates the start of the mesosphere.

taken from the 12-box model output (Western et al., 2025a, 2025b), using a reported total chlorine removing contributions from CH_3Cl, CH_2Cl_2, $CHCl_3$, CFC-13, CFC-114, CFC-115, HCFC-124 and adding a fixed 0.7 ppb offset to best match NOAA values. We computed a modified Cl_{tot} at three altitudes: 0–15 km ($Cl_{tot}^{0–15}$), 20–61 km ($Cl_{tot}^{20–61}$) and 0–61 km ($Cl_{tot}^{0–61}$) by excluding Cl-VSLS species (C_2Cl_4, CH_2Cl_2, $CHCl_3$, $C_2H_4Cl_2$) and CH_3Cl. The exclusion of CH_3Cl, in particular, was motivated by its rapidly changing profile in the lower troposphere. Applying a 0.62 ppb offset (instead of 0.7 ppb) to $Cl_{tot}^{0–15}$ shows strong agreement with both NOAA and AGAGE values (upper panel, Figure 8). Their fitted trends are nearly identical (rounded to the nearest ppt/year): −15 ppt/year ($Cl_{tot}^{0–15}$), −15 ppt/year (NOAA) and −14 ppt/year (AGAGE). Given the change in VMRs among several species, particularly Cl-VSLS, it is reasonable that a single offset applied across a wide temporal region may require adjustment.

Above the tropopause (20–61 km), Cl-VSLS and CH_3Cl are expected to have largely decomposed into product species (Cl_p). As a result $Cl_{tot}^{20–61}$ should approximate Cl_{tot}, which it generally does, with respective trends of −8.2 and −8.7 ppt/year. A relatively consistent offset of approximately 0.1 ppb is observed between them. No adjustment was applied to $Cl_{tot}^{20–61}$, in contrast to the tropospheric $Cl_{tot}^{0–15}$ (orange) and NOAA (blue) series shown in Figure 8. As previously demonstrated, hemispheric differences in tropospheric chlorine in recent years mainly reflects Cl-VSLS variability. A least-squares linear fit to the 60–30°N $Cl_{tot}^{0–61}$ produces a trend of −10.20 ppt/year, which is consistent with the 30–60°S Cl_{tot} trend of −10.25 ppt/year (Table 5), as opposed to the 60–30°N Cl_{tot} trend of −8.72 ppt/year (Table 5), reinforcing this conclusion. Because CH_3Cl is relatively uniform with latitude, the remaining inter-dataset differences (between Cl_{tot} and $Cl_{tot}^{0–61}$) are attributed primarily to Cl-VSLS contributions. Agreement between NOAA and $Cl_{tot}^{0–61}$ is strong from 2004 to 2010 but weakens thereafter, with the largest divergence between 2019 and 2024.

Following our previous work on fluorine (Raymond et al., 2025), we generated an adjusted series that includes all species in this work not present in the global NOAA value (see Table 1). Because NOAA data were used as the reference for species with the largest contributions to ground-based total chlorine (CFC-11, CFC-12, CFC-113, CCl_4, CH_3Cl, HCFC-22) the adjustment was applied only to NOAA values. This ensures internal consistency between the major-species baselines and the adjusted series; comparable treatment of AGAGE data is deferred to future work, as well as any direct Cl_{tot} comparisons between NOAA- and AGAGE-based inventories. This adjustment ($Cl_{tot}(NOAA)^+$, brown line, Figure 8; listed as "Global (supplemented)" in Table 5) exhibits a trend of -9.54 ± 0.79 ppt/year, in strong agreement with our global Cl_{tot} trend of -9.56 ± 0.28 ppt/year. Adding a 0.2 ppb offset further improves agreement with NOAA values between 2005 and 2012, after which the two series diverge again, similar to the behavior of $Cl_{tot}^{0–15}$ and $Cl_{tot}^{20–61}$. In part, this discrepancy can be attributed to CH_3Cl variability, and the growing influence of Cl-VSLS in recent years. In the lower panel of Figure 8, relative differences between the series are shown, with Cl_{tot} (black) shifted by −0.1 ppb for clarity. A maximum difference of 210 ppt between Cl_{tot} and the NOAA value is observed in 2024. Modest enhancements in $Cl_{tot}^{20–61}$ in 2011, 2017, and 2023, are consistent with a recurring 6-year pattern, and may reflect the 5–7 years cycle of Brewer-Dobson Circulation (BDC; Mahieu et al., 2014; Prignon et al., 2021). Finally, the divergence of the Cl_{tot} $(NOAA)^+$ (brown) series beginning in 2013 aligns with the post-2012 increase in CFC-11 emissions first reported by (S. A. Montzka et al., 2018), and persists through 2019.

Table 6 compares 5-year Cl_{tot} trends in the 60–30°N band with those reported in Table 1-7 of the 2022 Ozone Assessment (WMO, 2022, Chapter 1, p. 91). The ACE-FTS total column (0–61 km) trends fall within the reported uncertainties for 2008–2016, but deviate for 2016–2020. Comparisons with tropospheric trends show reasonable agreement for 2008–2012, but significant deviations for 2012–2016 and 2016–2020. In part, these differences can be attributed to altitude and latitudinal factors, particularly the vertical profile of CH_3Cl. For completeness, we also report 5-year tropospheric Cl_{tot} trends excluding CH_3Cl, given its previously discussed rapid variability between 10 and 18 km, atypical vertical profile, and appreciable VMR (≈0.5 ppb), which accounts for roughly one-sixth of total tropospheric chlorine Overall, the comparison shows that ACE-FTS trends track ground-based chlorine declines up to 2016, but weaker post-2016 decreases possibly suggest slower upper-atmospheric adjustment relative to rapid near-surface changes. The mixed agreement across intervals points to unresolved variability in CH_3Cl, Cl-VSLS, and transient temporal events; quantifying their combined influence will be the focus of future work.

Table 2
Relative (%) Contribution of HCl to Cl_{tot}, VMR, and Associated Altitudes in 2005 and 2024

	2005			2024		
	Altitude (km)	% of Cl_{tot}	VMR (ppt)	Altitude (km)	% of Cl_{tot}	VMR (ppt)
82°N–60°N	16.5–61.5	22.4–98.8	770–3652	15.5–61.5	18.2–97.9	607–3505
60°N–30°N	17.5–61.5	19.2–98.7	654–3674	17.5–61.5	19.5–97.8	630–3483
30°N–30°S	21.5–61.5	22.2–98.6	793–3661	21.5–61.5	20.7–97.7	692–3455
30°S–60°S	16.5–61.5	19.1–98.7	654–3626	16.5–61.5	17.4–97.7	561–3424
60°S–82°S	13.5–61.5	17.5–98.7	592–3642	13.5–61.5	18.7–97.8	589–3451

Note. The lower altitude range is determined using a cutoff around 20% of Cl_{tot}.

A distinctive feature of this work is the broad vertical coverage (0–61 km) enabled by the combination of satellite (ACE-FTS, MLS), ground-based (NOAA, AGAGE) and model (TOMCAT) data. This comprehensive data set allows for direct comparison across the troposphere, stratosphere, and (lower) mesosphere altitude regions. For the 60–30°N latitude band (Figure 9, upper panel), these regions are partitioned as 0–13 km, 13–50 km, and 50–61 km, respectively. Stratospheric and mesospheric values are shifted by 2 and 4 years, respectively, to account for age-of-air (AoA) effects. These values represent a possible underestimate of the true AoA, but were selected to maintain consistency with TOMCAT AoA estimates associated with the corresponding data used for profile extension. In practice, AoA can vary substantially, with plausible ranges of 2–6 years in the stratosphere and 4–9 years in the mesosphere, depending on transport pathways, vertical grid (pressure/altitude), seasonality, and interannual variability. Recent analysis of ACE-FTS SF_6 measurements (Saunders et al., 2025) suggests that the true AoA may be higher than assumed here, implying that our choice is conservative. Nevertheless, the use of fixed values ensures internal consistency within the analysis and is reasonable for investigating annual trends.

Table 3
Relative (%) Contributions of CFC-11, CFC-12, and Their Combined Contribution to Cl_{tot}, Effective VMR (Section 3), and Associated Altitudes in 2005 and 2024

	2005			2024		
	Altitude (km)	% of Cl_{tot}	Effective VMR (ppt)	Altitude (km)	% of Cl_{tot}	Effective VMR (ppt)
CFC-11						
82°N–60°N	0.5–12.5	21.9–20.4	751–683	0.5–4.5	19.9–20.0	645–640
60°N–30°N	0.5–13.5	21.6–20.1	751–685	0.5–7.5	19.5–19.8	645–641
30°N–30°S	0.5–18.5	22.2–20.1	747–692	0.5–6.5	20.5–20.3	643–632
30°S–60°S	0.5–13.5	22.4–20.2	745–680	0.5–12.5	21.0–20.0	642–606
60°S–82°S	0.5–12.5	22.4–19.4	745–646	0.5–10.5	21.2–19.9	642–621
CFC-12						
82°N–60°N	0.5–18.5	31.7–20.7	1086–697	0.5–17.5	29.7–21.0	963–664
60°N–30°N	0.5–20.5	31.3–19.3	1086–683	0.5–19.5	29.1–19.8	963–640
30°N–30°S	0.5–26.5	32.1–19.5	1081–688	0.5–25.5	30.7–20.8	964–687
30°S–60°S	0.5–19.5	32.5–18.9	1080–654	0.5–19.5	31.5–20.0	964–639
60°S–82°S	0.5–16.5	32.5–20.3	1080–689	0.5–16.5	31.8–19.9	964–633
Total						
82°N–60°N	0.5–20.5	53.6–21.4	1837–760	0.5–20.5	49.6–19.4	1607–648
60°N–30°N	0.5–22.5	52.9–18.9	1837–702	0.5–21.5	48.6–21.1	1607–727
30°N–30°S	0.5–27.5	54.3–20.9	1828–743	0.5–27.5	51.2–19.9	1607–664
30°S–60°S	0.5–21.5	54.9–19.3	1824–708	0.5–21.5	52.5–21.2	1606–724
60°S–82°S	0.5–19.5	55.0–18.4	1824–646	0.5–18.5	52.9–21.5	1606–680

Note. The upper altitude range is determined using a cutoff around 20% of Cl_{tot}.

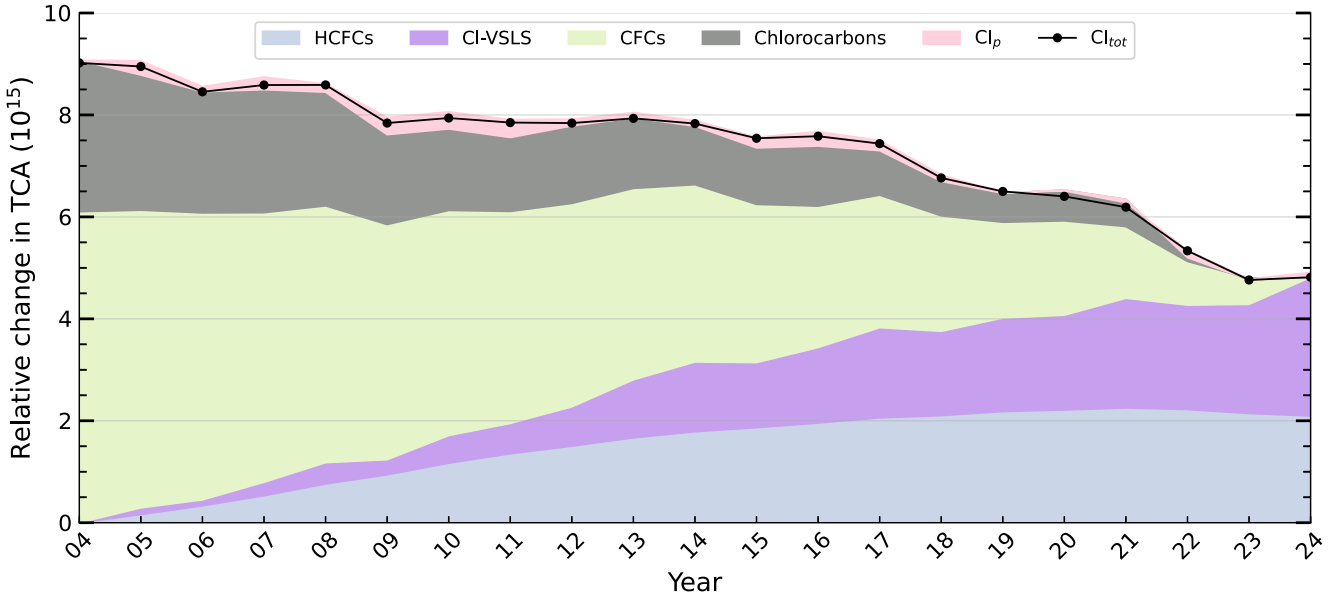

Figure 6. Stacked area plot showing the relative change in weighted total column abundance (TCA; molecules/cm^2) from 2004 to 2024 for four groups of chlorine source species (see Table 1) in the 60–30°N latitude band. The Chlorocarbon group is defined as CCl_4, CH_3Cl and CH_3CCl_3. The Cl-VSLS group contains C_2Cl_4, CH_2Cl_2, $CHCl_3$, and 1,2-DCA. The change in abundance for each group is calculated relative to its lowest annual value between 2004 and 2024. Abundances are weighted by the number of chlorine atoms per molecule. The TCA of Cl_{tot} is computed and plotted independently, and shows good agreement with the changes in the grouped source species abundances. A clear increase in Cl-VSLS and HCFCs is evident in recent years, along with a continued decrease in CFCs, consistent with the effects of the Montreal Protocol.

A bias of approximately 0.1 ppb is observed between the mesospheric and stratospheric mean Cl_{tot} across all latitude bands (Figure 9, lower panel). This offset is larger than would be expected based on AoA considerations alone (using TOMCAT-based AoA values), but its exact cause cannot be determined. Several factors may contribute, including (a) a slight high bias in ACE-FTS HCl at the upper end of the retrieval altitude range, (b) an underestimate of the assumed AoA values or (c) a slight underestimation of stratospheric Cl_{tot} rather than overestimation in the mesosphere. The apparent bias is smaller than the estimated uncertainty in mesospheric Cl_{tot} (~200–300 ppt) and therefore lies within expected measurement variability. Additional differences in chlorine partitioning and uncertainties in ClO measurements in the upper altitude region (40–60 km), particularly around 35 km where multiple chlorine-containing species are present, may also contribute. After accounting for the bias (Figure 9, upper panel), the three altitude regions show good agreement within one standard deviation. The primary contributions above 50 km are HCl and HCFC-22.

The lower panel of Figure 9 compares the mean Cl_{tot} for each latitude band and altitude region. A clear overlap is evident between the Northern Hemisphere (30–82°N) tropospheric Cl_{tot} (purple and blue) and the stratospheric Cl_{tot} across all latitude bands, while latitudinal differences in the mesosphere remain small (less than 50 ppt for all

Table 4
Relative (%) Contribution of Cl-VSLS to Cl_{tot}, Effective VMR (Section 3), and Associated Altitudes in 2005 and 2024

	2005			2024		
	Altitude (km)	% of Cl_{tot}	Effective VMR (ppt)	Altitude (km)	% of Cl_{tot}	Effective VMR (ppt)
82°N–60°N	0.5–15.5	3.5–1.4	121–49	0.5–15.5	7.6–3.3	246–111
60°N–30°N	0.5–15.5	3.4–2.0	119–70	0.5–15.5	7.7–4.7	254–161
30°N–30°S	0.5–15.5	2.0–1.8	67–64	0.5–15.5	3.6–3.3	114–109
30°S–60°S	0.5–15.5	1.4–0.8	47–26	0.5–15.5	2.4–1.4	75–45
60°S–82°S	0.5–15.5	1.4–0.3	47–11	0.5–15.5	2.4–0.5	73–17

Note. The altitude range is fixed above at 15 km.

Table 5
Annual Trends in Average Total Chlorine (Cl_{tot}) VMR (ppt), Between 2004 and 2024 for Each Latitude Band

Region	ppt/year	%/year
ACE-FTS		
82°N–60°N	−9.03 ± 0.25	−0.262 ± 0.007
60°N–30°N	−8.72 ± 0.29	−0.254 ± 0.009
30°N–30°S	−10.49 ± 0.27	−0.309 ± 0.008
30°S–60°S	−10.40 ± 0.29	−0.307 ± 0.009
60°S–82°S	−10.10 ± 0.29	−0.296 ± 0.009
Northern Hemisphere	−8.88 ± 0.27	−0.26 ± 0.01
Southern Hemisphere	−10.25 ± 0.29	−0.30 ± 0.01
Global (ACE-FTS)	−9.56 ± 0.28	−0.28 ± 0.01
Ground-based		
Global (NOAA)	−15.01 ± 0.35	–
Global (AGAGE)	−13.99 ± 0.27	–
Global (supplemented)	−9.54 ± 0.79	–

Note. %/year is not reported for ground-based VMRs as the magnitude of Cl_{tot} is different such that directly comparing to ACE-FTS is misleading. Listed uncertainties are the standard errors of the least-squares trend estimates.

years). Mesospheric Cl_{tot} decreases from 2004 to 2013, plateaus between 2013 and 2019 at ≈3.5 ppb, followed by a further decline until 2024, when Northern latitudes show an anomalous increase. Over the full period, mesospheric Cl_{tot} decreases by 0.2 ppb (from 3.65 to 3.45 ppb), while stratospheric Cl_{tot} declines steadily from ≈3.5 to 3.3 ppb. The overlap of the 60–30°N and 82–60°N tropospheric bands with the stratosphere Cl_{tot} across all latitude bands reflecting the dominant influence of Northern Hemisphere emissions.

As discussed earlier in relation to the 5–7 years BDC cycle, Figure 8 shows a recurring enhancement approximately every 6 years, most apparent in 2011, 2017, and 2023. Although minor, the stratospheric mean Cl_{tot} in Figure 9 appears to exhibit a maximal spread among latitude bands during these years. The largest deviation occurs between the 30°N–30°S and 82–60°N bands. This difference may be consistent with the effects of the Brewer-Dobson Circulation (BDC), which is biased toward the Northern Hemisphere (Butchart, 2014).

4.5. Radiative Efficiency-Weighted Chlorine Budget Trends

The chlorine species considered in this work include greenhouse gases and those with substantial radiative effects. To evaluate their impact, Cl_{tot} was weighted using the radiative efficiency (RE) of each individual species

$$RF_i = RE_i \times VMR_i \quad (2)$$

to calculate the change in RF due to changes in the VMRs of chlorine-containing molecules between 2004 and 2024. For each latitude band and year, RF values were calculated in the same manner as Cl_{tot}, as described in the previous work (Raymond et al., 2025). RE values were obtained from the "well-mixed" column (third from left) of Table A-5 (p. 449) in the 2022 Ozone Assessment (WMO, 2022). Values are listed on the odd-numbered pages. Adjustments included in the RE values are described in Section A.2.5 (p. 443) of (WMO, 2022). Temporal trends in RF for each latitude band are summarized in Table S8 and Figure S20 of Supporting Information S1.

In Figure 10, the normalized evolution of RF is shown for each species over the 2004–2024 period. A species-specific baseline correction is applied by subtracting the minimum RF value over 2004–2024 from each series. Thus, declining species (e.g., CFCs) are shifted so that their 2024 value is zero, whereas increasing species (e.g., HCFCs) are shifted so that their 2004 value is zero. This approach highlights the temporal evolution of individual species rather than their absolute contributions. The black line (Cl_{tot}) represents the total RF

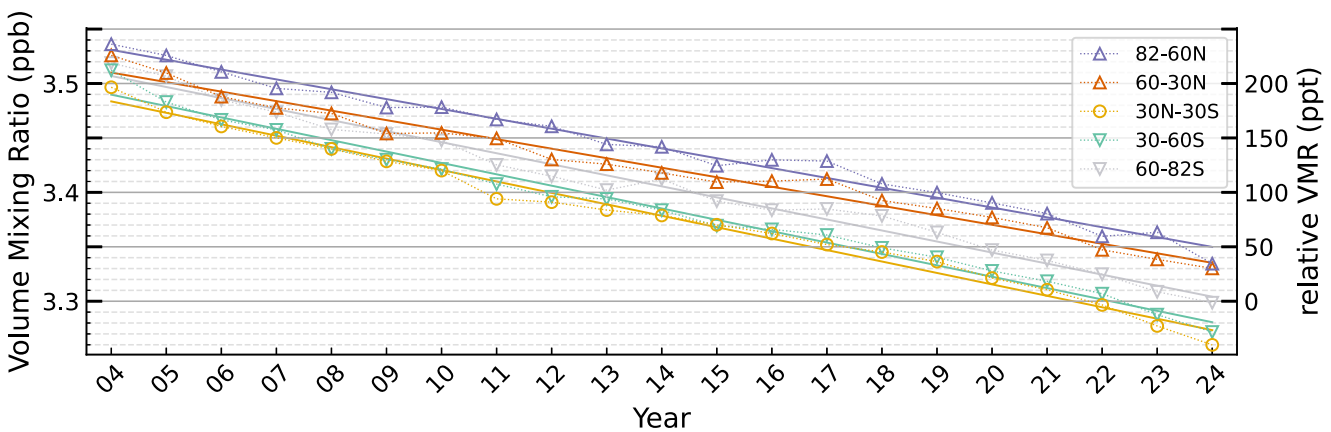

Figure 7. Mean total chlorine (Cl_{tot}) VMR (ppb) from 2004 to 2024 for each latitude band. The uncertainty of Cl_{tot} (not shown) is represented by the standard deviation of the mean for each individual year, between 130 and 170 ppt. The dashed lines connect the annual mean data, and the solid lines show the corresponding linear least-squares fit for each latitude band. The secondary *y*-axis on the right displays the relative difference in VMR with respect to the 2024 Cl_{tot} value for the 60–82°S latitude band.

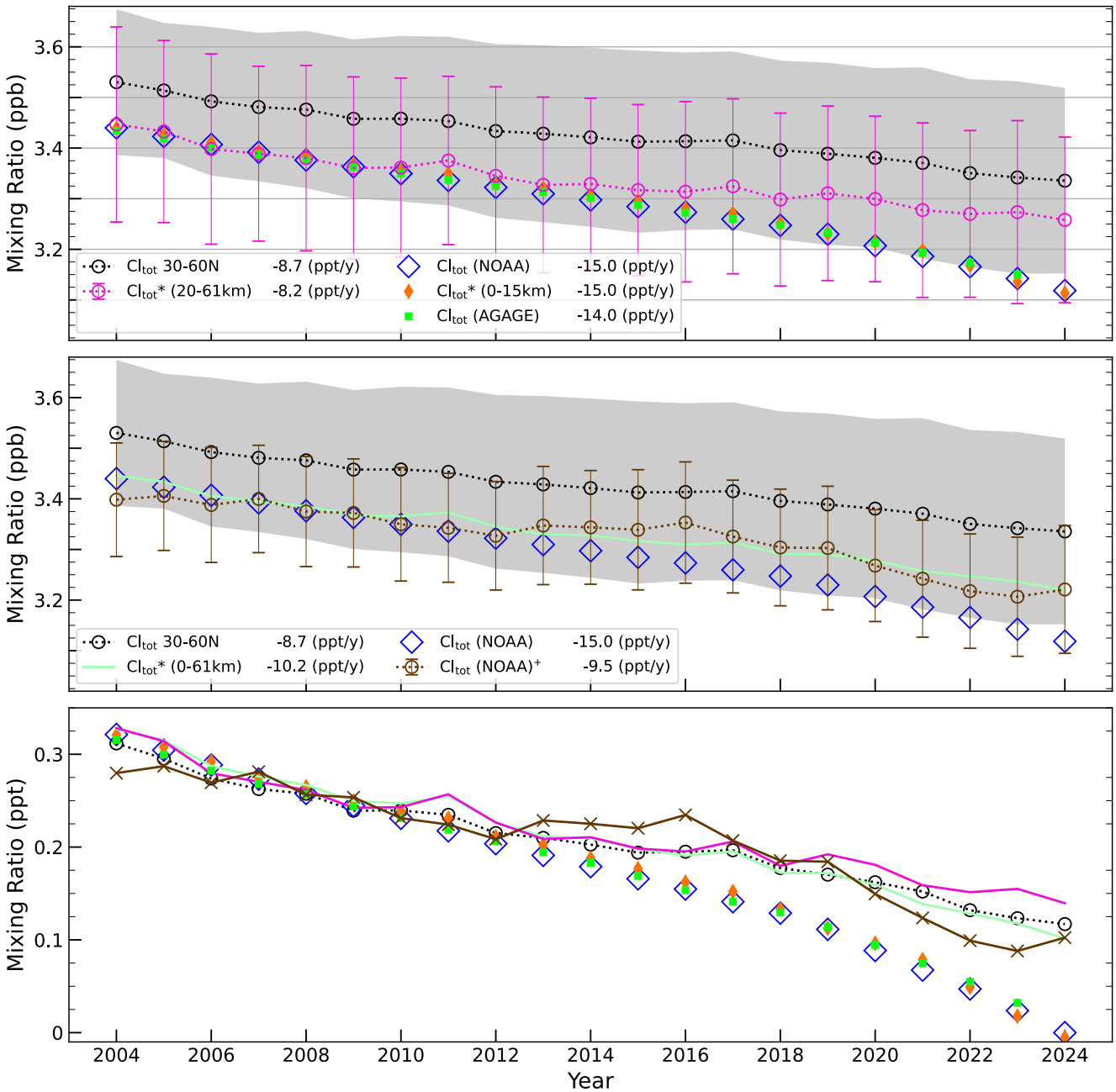

Figure 8. Comparison of calculated mean total chlorine (Cl_{tot}) VMR (ppb) (black) with average of reported ground-based values from NOAA (blue) and AGAGE (lime green) from 2004 to 2024 for the 60–30°N latitude band. Cl_{tot}^{0-15}, Cl_{tot}^{20-61}, and Cl_{tot}^{0-61} represent calculated means excluding the Cl-VSLS (C_2Cl_4, CH_2Cl_2, $CHCl_3$, $C_2H_4Cl_2$) and CH_3Cl across three altitudes ranges: 0–15 km, 20–61 km, and 0–61 km, respectively. For each data set the annual trend, a linear least-squares best fit, is listed in the legend. The upper panel compares total chlorine trends from ground-based measurements (NOAA, AGAGE) with ACE-FTS values representing the troposphere (orange), upper atmosphere (fuchsia), and full altitude range (black). The middle panel contrasts the adjusted NOAA series (brown) and ACE-FTS values both with and without Cl-VSLS. The lower panel presents all series expressed relative to the 2024 NOAA (blue) value, with Cl_{tot} (black) shifted downward by 0.1 ppb for clarity; all other series are equivalent to the previous two panels. As explained in the main text, constant offsets of 0.7, 0.62, and 0.2 ppb were applied to Cl_{tot} (NOAA), Cl_{tot}^{0-15}, and Cl_{tot} $(NOAA)^+$, in the upper and middle panels, respectively. Colored envelopes and error bars denote the uncertainty of Cl_{tot} as the standard deviation of the mean. The uncertainty of mean Cl_{tot} using NOAA or AGAGE data (not shown) is no more than 9 ppt for all years. The uncertainty of Cl_{tot}^{0-15} (not shown) ranges from 25 to 50 ppt over all years.

contribution from all species, referenced to its 2024 value and shifted upward by ≈ 21 mW/m^2 so that the 2024 point aligns with the upper boundary of the shaded regions. This adjustment facilitates comparison between the total and the component series but does not affect relative differences among species.

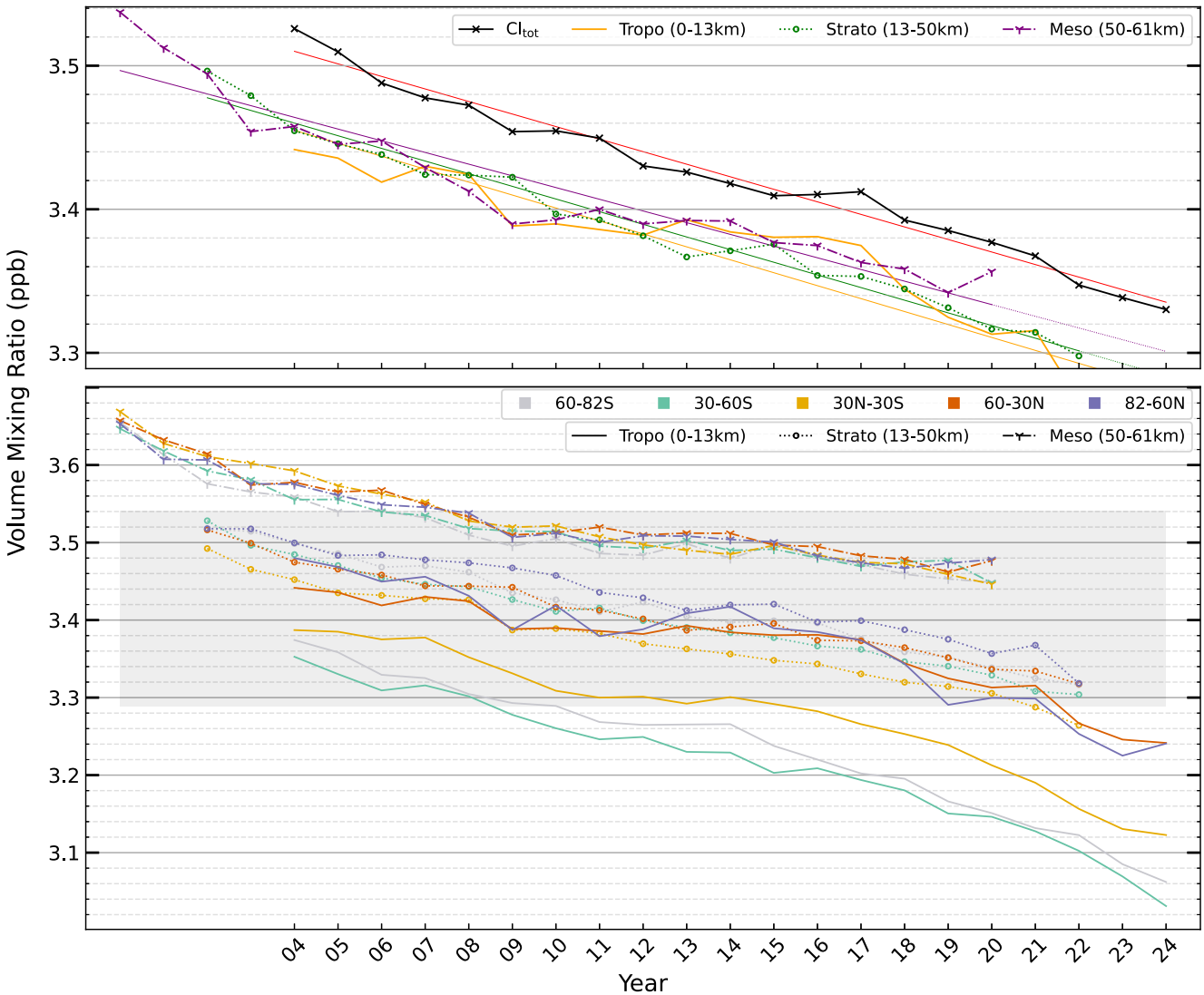

Figure 9. Comparison of calculated mean total chlorine (Cl_{tot}) VMR (ppb) for the five latitude bands and three altitude regions from 2004 to 2024. A shift of 2 years for the stratosphere and 4 years for the mesosphere is applied to account for age-of-air (AoA). The upper panel compares the 60°N–30°N latitude band, with stratospheric and mesospheric VMRs offset by −20 ppt and −120 ppt, respectively, for visual comparison (see text). Solid thin lines represent linear least-squares best fits, with extrapolated points shown as dotted lines. Uncertainties (not shown) are 124–142 ppt for the troposphere, 127–176 for the stratosphere, 161–282 ppt for the mesosphere and 133–187 ppt for Cl_{tot}. The lower panel compares all latitude bands, with a gray shaded region indicating the range of the upper panel. Uncertainty is not shown but is similar, across latitude bands, to uncertainty shown for the 60°N–30°N band. A similar shift of 2 and 4 years is applied in the lower panel, but without any adjustment to the VMR.

Reasonable agreement is found between our absolute RF values (Figure S21 in Supporting Information S1) and those reported in the 2022 Ozone Assessment (WMO, 2022, Chapter 1). For example, we calculate an absolute RF of 256.2 mW/m^2 for CFCs in 2020, compared to 257 mW/m^2 reported in the Ozone Assessment. In relative terms (Figure 10), CFC-related RF decreases steadily throughout the record, while HCFC-22 increases until about 2018 and then appears to have plateaued. After 2018, year-to-year variations in HCFC-22 RF are within the estimated uncertainty, consistent with a broad plateau extending into the early 2020s and with reported global mean maxima near 2021 (Western et al., 2024). The total RF values remain largely consistent from 2004 to 2014, followed by a gradually decline until 2018. From 2018 to 2024 total RF decreases by ≈15 mW/m^2, the bulk of the ≈22 mW/m^2 loss between 2004 and 2024. The majority of the absolute RF contribution is due to CFCs, accounting for 81% (≈281 of 347 mW/m^2) in 2004 and decreasing to 75% (≈ 245 of 325 mW/m^2) in 2024, primarily CFC-11 and CFC-12. The increasing contribution from HCFC-22 seems to offset the decline in CFCs until 2018; however, HCFC-

Table 6
Comparison of Five-Year Linear Trends (ppt/Year) in Cl_{tot} for the 60–30°N Band, Derived From ACE-FTS, With the "Average Rate of Change of Total Cl" Reported in Table 1-7 of the 2022 Ozone Assessment (WMO, 2022)

60–30°N	2008–2012	2012–2016	2016–2020	2020–2024
Ozone Assessment	−12.1 ± 8.0	−3.6 ± 4.7	−15.1 ± 3.6	–
(0–61 km) ACE	−8.7 ± 1.9	−5.6 ± 0.9	−9.2 ± 1.6	−12.2 ± 1.2
(0–13 km) ACE	−8.7 ± 3.7	−1.4 ± 1.6	−18.6 ± 2.0	−21.3 ± 4.4
(0–13 km) ACE*	−11.1 ± 1.7	−2.9 ± 2.1	−17.8 ± 2.1	−14.5 ± 4.6
(0 km) NOAA	−13.5 ± 0.1	−12.3 ± 0.2	−16.2 ± 1.2	−22.1 ± 0.4
(0 km) AGAGE	−12.6 ± 0.1	−13.1 ± 0.5	−14.5 ± 0.9	−20.7 ± 0.5

Note. Results are shown for the full ACE total column (0–61 km), a tropospheric subset (0–13 km), and a version excluding CH_3Cl (denoted by an asterisk) to illustrate the sensitivity of derived trends to its tropospheric profile. Ground-based series (NOAA, AGAGE) are included for comparison at the surface. (Quoted uncertainty values represent the standard error from linear regression, and should not be interpreted as full measurement uncertainties for NOAA and AGAGE.)

22's RF contribution appears to have plateaued in recent years. As a result, a more pronounced decline in RF is observed in recent years, with respect to the species examined in this study.

5. Concluding Remarks

In this work ACE-FTS measurements of 13 chlorine-containing molecules, in the atmosphere from 2004 to 2024, are presented. Ground-based observations, Aura Microwave Limb Sounder (MLS) data, and TOMCAT model data were employed to complement these measurements. Vertical profiles of product (Cl_p), source (Cl_s) and total chlorine (Cl_{tot}) were calculated for five latitude bands (82–60°N, 60–30°N, 30°N–30°S, 30–60°S, and 60–82°S) over 21 years (2004–2024). Assessing the relative (%) contribution of individual species to Cl_{tot} showed evidence of Cl-VSLS and HCFC-22 slowing the reduction in atmospheric chlorine by way of Montreal Protocol controls on CFCs and other gases, such as methyl chloroform (CH_3CCl_3) and carbon tetrachloride (CCl_4). The global yearly trend of Cl_{tot} was determined to be −0.28%/year or −9.56 ppt/year, aligning well with the decrease observed in ground-based measurements over 21 years (0.2–0.25 ppb) (3.5 → 3.3 ppb). Comparison of different atmospheric regions revealed the increasing influence of Cl-VSLS on total atmospheric chlorine. These contributions have partially mitigated the rate of Cl_{tot} decline, particularly in the Northern Hemisphere, highlighting a growing role for these species in shaping the chlorine budget. HCl remains the dominant contributor to Cl_{tot} in the upper stratosphere and mesosphere, while the lower stratosphere and troposphere remain influenced by CFCs, HCFCs, and chlorocarbons. An apparent high bias of approximately 0.1 ppb was observed when comparing average mesospheric Cl_{tot} and stratospheric Cl_{tot} values. Weighting the global yearly trend of Cl_{tot} by radiative efficiency (RE) showed good agreement with radiative forcing (RF) values reported in the 2022 Ozone Assessment. Analysis of RF trends revealed that the decrease from 2018 to 2024 was greater than that over the full 2004–2024 period, primarily due to changes in the VMR of HCFC-22.

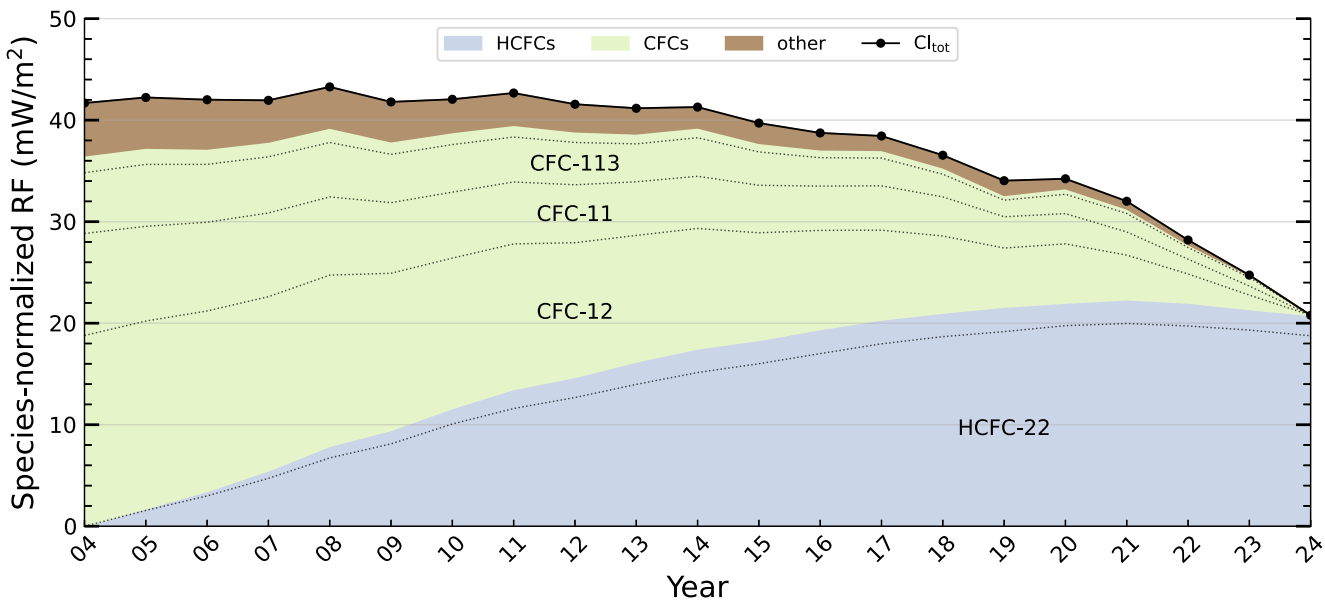

Figure 10. Mean radiative forcing (RF; mW/m^2) between 2004 and 2024 in the 60–30°N latitude band. Colored regions show each species' RF normalized (i.e., expressed relative) to its minimum value during 2004–2024. The black line represents the total RF (sum of all species), referenced to its 2024 value and shifted upward so that the 2024 point aligns with the upper boundary of the shaded regions. The total RF (black line) declined by ≈ 21 mW/m^2 between 2004 and 2024, with relative contributions from HCFCs and CFCs changing in opposing directions. Uncertainty, not shown, is 1 standard deviation of the mean RF, approximately 10 mW/m^2 for all years and latitudes. Calculations were limited to the altitude range below representative tropopause heights for the latitude region (16 km).

ACE's high-resolution Fourier transform spectrometer allows for retrievals of a wide variety of atmospheric species, without which this work would not have been possible. ACE provides information on altitude variations of chlorine-containing molecules, which ground-based measurements cannot. ACE represents one of few sources of multi-decade satellite measurements for key species generated in the stratosphere such as HCl and $ClONO_2$, which together account for more than 90% of Cl_{tot} in the middle to upper stratosphere. Sustaining long-term, vertically resolved measurements offer a potential pathway for detecting future shifts in halogen budgets as both regulated and unregulated species evolve. With over two decades of measurements, ACE continues to provide high quality atmospheric data, supporting critical climate and ozone research. The ongoing operation of ACE provides a valuable long-term record of atmospheric chlorine chemistry, important in understanding the trajectory and mechanisms of ozone recovery. These findings further demonstrate the effectiveness of the Montreal Protocol, while also highlighting the need for continued monitoring of CFCs, HCFCs, and emerging chlorine sources such as Cl-VSLS.

Conflict of Interest

The authors declare no conflicts of interest relevant to this study.

Data Availability Statement

ACE-FTS version 5.3 retrieval results and ACE-imager extinction profiles are freely available from the ACE web portal: https://databace.scisat.ca/level2/ace_v5.3/display_data.php (ACE-SOC, 2025). Initial registration is required at: https://databace.scisat.ca/l2signup.php. TOMCAT model data, together with the calculated mean Cl_{tot} VMRs and corresponding uncertainties, are available at https://doi.org/10.5281/zenodo.17612886 (Raymond, 2025). NOAA data was obtained from their GML, publicly available online: https://gml.noaa.gov/dv/data/ (NOAA-GML, 2025), or https://gml.noaa.gov/hats/data.html (NOAA-LOGOS, 2025). Data for NOAA Chlorine Trends was obtained from https://gml.noaa.gov/aftp/data/hats/Total_Cl_Br/, with 2024 data provided by Stephen Montzka. Files for each species were downloaded individually, such as the CFC-11 HATS combined file at https://gml.noaa.gov/aftp/data/hats/cfcs/cfc11/combined/HATS_global_F11.txt (Dutton et al., 2025). The most recent AGAGE observations are available at (AGAGE-data, 2025; Prinn, Weiss, Arduini, Choi, et al., 2024). The data set employed in this study was retrieved from (AGAGE-data, 2024); however, that location is no longer accessible, so (Prinn, Weiss, Arduini, Arnold, et al., 2024) serves as an alternative source for similar AGAGE data. All measurements from AGAGE were obtained in a single tar file.

Acknowledgments

The ACE mission is funded by the Canadian Space Agency, Canada (9F045-230412/001). Some support was provided by NASA through the Atmospheric Composition Modeling and Analysis Program (80NSSC23K0999). The modelling work at Leeds was supported by NERC Grants NE/V011863/1 and NE/X003450/1. AGAGE is supported principally by the National Aeronautics and Space Administration (USA) grants to the Massachusetts Institute of Technology and the Scripps Institution of Oceanography. PB acknowledges RFB for productive discussion. We thank Stephen Montzka for help with citations and providing updated NOAA data. We thank Cathy Trudinger, Luke Western and Jens Mühle for providing global total chlorine calculated from the AGAGE 12-box modelled abundances. The author acknowledges Lavinia Toso for stimulating exchanges and for her willingness to engage in extended discussions on multiple aspects of the subject.

References

ACE-SOC. (2025). Atmospheric Chemistry Experiment (ACE) Version 5.3 retrievals dataset [Dataset]. Retrieved from https://databace.scisat.ca/level2/ace_v5.3/display_data.php. Initial registration is required at: https://databace.scisat.ca/l2signup.php

AGAGE. (2025). Advanced global atmospheric gases experiment. Retrieved from https://tolnet.larc.nasa.gov/missions/agage/

AGAGE-data. (2024). AGAGE data [Dataset]. Retrieved from https://agage2.eas.gatech.edu/data_archive/agage/

AGAGE-data. (2025). AGAGE data [Dataset]. Retrieved from https://www-air.larc.nasa.gov/missions/agage/data/version-history/

Arosio, C., Chipperfield, M. P., Rozanov, A., Weber, M., Dhomse, S., Feng, W., et al. (2024). Investigating zonal asymmetries in stratospheric ozone trends from satellite limb observations and a chemical transport model. *Journal of Geophysical Research: Atmospheres*, *129*(8), e2023JD040353. https://doi.org/10.1029/2023JD040353

Bednarz, E. M., Hossaini, R., Chipperfield, M. P., Abraham, N. L., & Braesicke, P. (2022). Atmospheric impacts of chlorinated very short-lived substances over the recent past–Part 1: Stratospheric chlorine budget and the role of transport. *Atmospheric Chemistry and Physics*, *22*(16), 10657–10676. https://doi.org/10.5194/acp-22-10657-2022

Bernath, P. (2017). The Atmospheric Chemistry Experiment (ACE). *Journal of Quantitative Spectroscopy and Radiative Transfer*, *186*, 3–16. https://doi.org/10.1016/j.jqsrt.2016.04.006

Boone, C., Bernath, P., & Lecours, M. (2023). Version 5 retrievals for ACE-FTS and ACE-imagers. *Journal of Quantitative Spectroscopy and Radiative Transfer*, *310*, 108749. https://doi.org/10.1016/j.jqsrt.2023.108749

Bray, C., Tran, H., Jacquemart, D., & Lacome, N. (2012). Line mixing in ^{Q}Q sub branches of the ν_1 band of methyl chloride. *Journal of Quantitative Spectroscopy and Radiative Transfer*, *113*(17), 2182–2188. https://doi.org/10.1016/j.jqsrt.2012.07.026

Brown, A., Chipperfield, M., Dhomse, S., Boone, C., & Bernath, P. (2013). Global stratospheric chlorine inventories for 2004–2009 from Atmospheric Chemistry Experiment Fourier Transform Spectrometer (ACE-FTS) measurements. *Atmospheric Chemistry and Physics Discussions*, *13*(9), 23491–23548. https://doi.org/10.5194/acpd-13-23491-2013

Brune, W., Toohey, D., Lloyd, S., & Anderson, J. (1990). The sunrise and sunset variation of ClO in the lower stratosphere. *Geophysical Research Letters*, *17*(4), 509–512. https://doi.org/10.1029/GL017i004p00509

Butchart, N. (2014). The Brewer-Dobson circulation. *Reviews of Geophysics*, *52*(2), 157–184. https://doi.org/10.1002/2013RG000448

Chipperfield, M. (1999). Multiannual simulations with a three-dimensional chemical transport model. *Journal of Geophysical Research*, *104*(D1), 1781–1805. https://doi.org/10.1029/98JD02597

Chipperfield, M. P., Hossaini, R., Montzka, S. A., Reimann, S., Sherry, D., & Tegtmeier, S. (2020). Renewed and emerging concerns over the production and emission of ozone-depleting substances. *Nature Reviews Earth & Environment*, *1*(5), 251–263. https://doi.org/10.1038/s43017-020-0048-8

Chirkov, M., Stiller, G. P., Laeng, A., Kellmann, S., vonClarmann, T., Boone, C. D., et al. (2016). Global HCFC-22 measurements with MIPAS: Retrieval, validation, global distribution and its evolution over 2005–2012. *Atmospheric Chemistry and Physics*, *16*(5), 3345–3368. https://doi.org/10.5194/acp-16-3345-2016

Connor, B. J., Mooney, T., Barrett, J., Solomon, P., Parrish, A., & Santee, M. (2007). Comparison of ClO measurements from the aura Microwave Limb Sounder to ground-based microwave measurements at Scott base, Antarctica, in spring 2005. *Journal of Geophysical Research*, *112*(D24). https://doi.org/10.1029/2007JD008792

Dhomse, S. S., Chipperfield, M. P., Feng, W., Hossaini, R., Mann, G. W., Santee, M. L., & Weber, M. (2022). A single-peak-structured solar cycle signal in stratospheric ozone based on Microwave Limb Sounder observations and model simulations. *Atmospheric Chemistry and Physics*, *22*(2), 903–916. https://doi.org/10.5194/acp-22-903-2022

Dubé, K., Tegtmeier, S., Bourassa, A., Laube, J. C., Engel, A., Saunders, L. N., & Bednarz, E. M. (2025). Chlorinated very short-lived substances offset the long-term reduction of inorganic stratospheric chlorine. *Communications Earth & Environment*, *6*(1), 487. https://doi.org/10.1038/s43247-025-02478-9

Dutton, G., & Hall, B. (2023). Global atmospheric Halon-1211 hemispheric and global mean dry air mole fractions from the NOAA GML Halocarbons in situ network, 1998-2023, Version: 2023-08-29. https://doi.org/10.7289/V5X0659V

Dutton, G., Hall, B., Dlugokencky, E., Lan, X., Madronich, M., Nance, J., & Petersen, K. (2023). Combined atmospheric sulfur hexafluoride dry air mole fractions from the NOAA GML Halocarbons sampling network, 1995-2023, Version: 2023-08-30. https://doi.org/10.15138/TQ02-ZX42

Dutton, G., Hall, B., Montzka, S., Nance, J., Clingan, S., & Petersen, K. (2023a). Combined atmospheric carbon tetrachloride dry air mole fractions from the NOAA GML Halocarbons sampling network, 1995-2023, Version: 2023-08-30. https://doi.org/10.15138/CV0A-J604

Dutton, G., Hall, B., Montzka, S., Nance, J., Clingan, S., & Petersen, K. (2023b). Combined atmospheric chlorofluorocarbon-113 dry air mole fractions from the NOAA GML Halocarbons sampling network, 1992-2023, Version: 2023-08-29. https://doi.org/10.15138/4N0D-4M07

Dutton, G., Hall, B., Montzka, S., Nance, J., Clingan, S., & Petersen, K. (2023c). Combined atmospheric chlorofluorocarbon-11 dry air mole fractions from the NOAA GML Halocarbons sampling network, 1977-2023, Version: 2023-08-29. https://doi.org/10.15138/BVQ6-2S69

Dutton, G., Hall, B., Montzka, S., Nance, J., Clingan, S., & Petersen, K. (2023d). Combined atmospheric chlorofluorocarbon-12 dry air mole fractions from the NOAA GML Halocarbons sampling network, 1977-2023, Version: 2023-08-29. https://doi.org/10.15138/PJ63-H440

Dutton, G., Hall, B., Montzka, S., Nance, J., Clingan, S., & Petersen, K. (2025). Combined atmospheric chlorofluorocarbon-11 dry air mole fractions from the NOAA GML Halocarbons sampling network, 1977-2024, Version: 2024-09-26 [Dataset]. https://doi.org/10.15138/BVQ6-2S69

Fahey, D. W., & Hegglin, M. I. (2011). *Twenty questions and answers about the ozone layer: 2010 update* (p. 516). World Meteorological Organization. Retrieved from https://csl.noaa.gov/assessments/ozone/2010/twentyquestions/

Feng, W., Chipperfield, M. P., Dorf, M., Pfeilsticker, K., & Ricaud, P. (2007). Mid-latitude ozone changes: Studies with a 3-D CTM forced by ERA-40 analyses. *Atmospheric Chemistry and Physics*, *7*(9), 2357–2369. https://doi.org/10.5194/acp-7-2357-2007

Froidevaux, L., Kinnison, D. E., Santee, M. L., Millán, L. F., Livesey, N. J., Read, W. G., et al. (2021). Upper stratospheric ClO and HOCl trends (2005–2020): Aura microwave limb sounder and model results. *Atmospheric Chemistry and Physics Discussions*, *2021*(7), 1–42. https://doi.org/10.5194/acp-22-4779-2022

Harrison, J. J., Chipperfield, M. P., Boone, C. D., Dhomse, S. S., Bernath, P. F., Froidevaux, L., et al. (2016). Satellite observations of stratospheric hydrogen fluoride and comparisons with SLIMCAT calculations. *Atmospheric Chemistry and Physics*, *16*(16), 10501–10519. https://doi.org/10.5194/acp-16-10501-2016

Hersbach, H., Bell, B., Berrisford, P., Hirahara, S., Horányi, A., Muñoz-Sabater, J., et al. (2020). The ERA5 global reanalysis. *Quarterly Journal of the Royal Meteorological Society*, *146*(730), 1999–2049. https://doi.org/10.1002/qj.3803

Hossaini, R., Atlas, E., Dhomse, S. S., Chipperfield, M. P., Bernath, P. F., Fernando, A. M., et al. (2019). Recent trends in stratospheric chlorine from very short-lived substances. *Journal of Geophysical Research: Atmospheres*, *124*(4), 2318–2335. https://doi.org/10.1029/2018JD029400

Hossaini, R., Sherry, D., Wang, Z., Chipperfield, M. P., Feng, W., Oram, D. E., et al. (2024). On the atmospheric budget of 1,2-dichloroethane and its impact on stratospheric chlorine and ozone (2002–2020). *Atmospheric Chemistry and Physics*, *24*(23), 13457–13475. https://doi.org/10.5194/acp-24-13457-2024

Kawamoto, N., & Shiotani, M. (2000). Interannual variability of the vertical descent rate in the antarctic polar vortex. *Journal of Geophysical Research*, *105*(D9), 11935–11946. https://doi.org/10.1029/2000jd900076

Khalil, M., & Rasmussen, R. (1999). Atmospheric methyl chloride. *Atmospheric Environment*, *33*(8), 1305–1321. https://doi.org/10.1016/S1352-2310(98)00234-9

Khosravi, M., Baron, P., Urban, J., Froidevaux, L., Jonsson, A., Kasai, Y., et al. (2013). Diurnal variation of stratospheric and lower mesospheric equator: Comparison of 1-d model calculations with measurements by satellite instruments. *Atmospheric Chemistry and Physics*, *13*(15), 7587–7606. https://doi.org/10.5194/acp-13-7587-2013

Kreyling, D., Sagawa, H., Wohltmann, I., Lehmann, R., & Kasai, Y. (2013). Smiles zonal and diurnal variation climatology of stratospheric and mesospheric trace gasses: O_3, HCl, HNO_3, ClO, BrO, HOCl, H_2O, and temperature. *Journal of Geophysical Research: Atmospheres*, *118*(20), 11–888. https://doi.org/10.1002/2012JD019420

Lary, D. (1997). Catalytic destruction of stratospheric ozone. *Journal of Geophysical Research*, *102*(D17), 21515–21526. https://doi.org/10.1029/97JD00912

Livesey, N., Read, W., Wagner, P., Froidevaux, L., Santee, M., Schwartz, M., et al. (2022). *Earth Observing System (EOS) Aura Microwave Limb Sounder (MLS) version 5.0x level 2 and 3 data quality and description document version 5.0–1.1 a* (Technical Report). Jet Propulsion Laboratory, California Institute of Technology. Retrieved from https://mls.jpl.nasa.gov/data/v5-0_data_quality_document.pdf

Ma, Q., & Boulet, C. (2021). Theoretical study of CH_3Cl-N_2 line shapes in the ν_1 band. Line mixing effects in QR doublets and QQ_k sub-branches. *Journal of Quantitative Spectroscopy and Radiative Transfer*, *273*, 107844. https://doi.org/10.1016/j.jqsrt.2021.107844

Mahieu, E., Chipperfield, M., Notholt, J., Reddmann, T., Anderson, J., Bernath, P., et al. (2014). Recent northern hemisphere stratospheric HCl increase due to atmospheric circulation changes. *Nature*, *515*(7525), 104–107. https://doi.org/10.1038/nature13857

McKenzie, R. L., Bernhard, G. H., Liley, B., Disterhoft, P., Rhodes, S., Bais, A. F., et al. (2019). Success of Montreal Protocol demonstrated by comparing high-quality UV measurements with "world avoided" calculations from two chemistry-climate models. *Scientific Reports*, *9*(1), 12332. https://doi.org/10.1038/s41598-019-48625-z

Molina, M. J. (1996). Role of chlorine in stratospheric chemistry. *Pure and Applied Chemistry*, *68*(9), 1749–1756. https://doi.org/10.1351/pac199668091749

Molina, M. J., & Rowland, F. S. (1974). Stratospheric sink for chlorofluoromethanes: Chlorine atom-catalysed destruction of ozone. *Nature*, *249*(5460), 810–812. https://doi.org/10.1038/249810a0

Montzka, S., Myers, R., Butler, J., & Elkins, J. (1994). Early trends in the global tropospheric abundance of hydrochlorofluorocarbon-141b and 142b. *Geophysical Research Letters*, *21*(23), 2483–2486. https://doi.org/10.1029/94GL02342

Montzka, S., Myers, R., Butler, J., Elkins, J., & Cummings, S. (1993). Global tropospheric distribution and calibration scale of HCFC-22. *Geophysical Research Letters*, *20*(8), 703–706. https://doi.org/10.1029/93GL00753

Montzka, S. A., Dutton, G. S., Portmann, R. W., Chipperfield, M. P., Davis, S., Feng, W., et al. (2021). A decline in global CFC-11 emissions during 2018-2019. *Nature*, *590*(7846), 428–432. https://doi.org/10.1038/s41586-021-03260-5

Montzka, S. A., Dutton, G. S., Yu, P., Ray, E., Portmann, R. W., Daniel, J. S., et al. (2018). An unexpected and persistent increase in global emissions of ozone-depleting CFC-11. *Nature*, *557*(7705), 413–417. https://doi.org/10.1038/s41586-018-0106-2

Nassar, R., Bernath, P., Boone, C. D., Clerbaux, C., Coheur, P.-F., Dufour, G., et al. (2006). A global inventory of stratospheric chlorine in 2004. *Journal of Geophysical Research*, *111*(D22). https://doi.org/10.1029/2006JD007073

Nedoluha, G. E., Connor, B. J., Mooney, T., Barrett, J. W., Parrish, A., Gomez, R. M., et al. (2016). 20 years of ClO measurements in the antarctic lower stratosphere. *Atmospheric Chemistry and Physics*, *16*(16), 10725–10734. https://doi.org/10.5194/acp-16-10725-2016

NOAA. (2025). NOAA global monitoring laboratory. Retrieved from https://gml.noaa.gov/

NOAA-data. (2025). NOAA total inorganic chlorine and bromine dataset (Total_Cl_Br) [Dataset]. *NOAA Global Monitoring Laboratory*. Retrieved from https://gml.noaa.gov/aftp/data/hats/Total_Cl_Br/

NOAA-GML. (2025). NOAA's Global Monitoring Laboratory (GML) data finder [Dataset]. Retrieved from https://gml.noaa.gov/dv/data/

NOAA-LOGOS. (2025). NOAA's long-term Observations of Greenhouse gases and ozone-depleting substances (LOGOS) data [Dataset]. Retrieved from https://gml.noaa.gov/hats/data.html

Prignon, M., Chabrillat, S., Friedrich, M., Smale, D., Strahan, S., Bernath, P. F., et al. (2021). Stratospheric fluorine as a tracer of circulation changes: Comparison between infrared remote-sensing observations and simulations with five modern reanalyses. *Journal of Geophysical Research: Atmospheres*, *126*(19), e2021JD034995. https://doi.org/10.1029/2021JD034995

Prinn, R. G., Weiss, R. F., Arduini, J., Arnold, T., DeWitt, H. L., Fraser, P. J., et al. (2018). History of chemically and radiatively important atmospheric gases from the Advanced Global Atmospheric Gases Experiment (AGAGE). *Earth System Science Data*, *10*(2), 985–1018. https://doi.org/10.5194/essd-10-985-2018

Prinn, R. G., Weiss, R. F., Arduini, J., Arnold, T., Fraser, P. J., Ganesan, A. L., et al. (2024). The dataset of in-situ measurements of chemically and radiatively important atmospheric gases from the Advanced Global Atmospheric Gases Experiment (AGAGE) and affiliated stations (2024R1) [Dataset]. *Advanced Global Atmospheric Gases Experiment (AGAGE), ESS-DIVE repository*. https://doi.org/10.15485/2476540

Prinn, R. G., Weiss, R. F., Arduini, J., Choi, H., Engel, A., Fraser, P. J., et al. (2024). The dataset of in-situ measurements of chemically and radiatively important atmospheric gases from the Advanced Global Atmospheric Gases Experiment (AGAGE) and affiliated stations (Version 20250721) [Dataset]. *Advanced Global Atmospheric Gases Experiment (AGAGE), ESS-DIVE repository*. https://doi.org/10.60718/75d7-qe84

Raymond, N. (2025). ACE-FTS derived total atmospheric chlorine and TOMCAT model output (2004-2024) [Dataset]. *Zenodo*. https://doi.org/10.5281/zenodo.17612886

Raymond, N., Bernath, P., Boone, C. D., & Chipperfield, M. P. (2025). Twenty years of global stratospheric fluorine inventories from Atmospheric Chemistry Experiment Fourier transform spectrometer (ACE-FTS) measurements. *Journal of Geophysical Research: Atmospheres*, *130*(15), e2024JD042298. https://doi.org/10.1029/2024JD042298

Rotermund, M. K., Bense, V., Chipperfield, M. P., Engel, A., Grooß, J.-U., Hoor, P., et al. (2021). Organic and inorganic bromine measurements around the extratropical tropopause and lowermost stratosphere: Insights into the transport pathways and total bromine. *Atmospheric Chemistry and Physics*, *21*(20), 15375–15407. https://doi.org/10.5194/acp-21-15375-2021

Salawitch, R. J., McBride, L. A., Thompson, C. R., Fleming, E. L., McKenzie, R. L., Rosenlof, K. H., et al. (2022). *Twenty questions and answers about the ozone layer citation: 2022 update*. (Tech. Rep.). GAW Report No. 278 (p. 509). WMO. Retrieved from https://csl.noaa.gov/assessments/ozone/2022/twentyquestions/

Saunders, L. N., Walker, K. A., Stiller, G. P., von Clarmann, T., Haenel, F., Garny, H., et al. (2025). Age of air from ACE-FTS measurements of sulfur hexafluoride. *Atmospheric Chemistry and Physics*, *25*(7), 4185–4209. https://doi.org/10.5194/acp-25-4185-2025

Schmidt, M., Bernath, P., Boone, C., Lecours, M., & Steffen, J. (2024). Trends in atmospheric composition between 2004–2023 using version 5 ACE-FTS data. *Journal of Quantitative Spectroscopy and Radiative Transfer*, *325*, 109088. https://doi.org/10.1016/j.jqsrt.2024.109088

Simmonds, P. G., Rigby, M., McCulloch, A., O'Doherty, S., Young, D., Mühle, J., et al. (2017). Changing trends and emissions of hydrochlorofluorocarbons (HCFCs) and their hydrofluorocarbon (HFCs) replacements. *Atmospheric Chemistry and Physics*, *17*(7), 4641–4655. https://doi.org/10.5194/acp-17-4641-2017

Smith, K., Atlas, E., Apel, E. C., Blake, D. R., Dutton, G., Hornbrook, R. S., et al. (2024). Chloromethanes in the north American troposphere and lower stratosphere over the past two decades. *Geophysical Research Letters*, *51*(15), e2024GL108710. https://doi.org/10.1029/2024GL108710

Tegtmeier, S. (2019). Anthropogenic chlorine under watch. *Nature Geoscience*, *12*(2), 84–86. https://doi.org/10.1038/s41561-018-0282-6

UNEP. (2024). *Environmental consequences of interacting effects of changes in stratospheric ozone, ultraviolet radiation and climate: UNEP environmental effects assessment panel, update 2024*. United Nations Environment Programme.

Vollmer, M. K., Mühle, J., Henne, S., Young, D., Rigby, M., Mitrevski, B., et al. (2021). Unexpected nascent atmospheric emissions of three ozone-depleting hydrochlorofluorocarbons. *Proceedings of the National Academy of Sciences*, *118*(5), e2010914118. https://doi.org/10.1073/pnas.2010914118

Vollmer, M. K., Young, D., Trudinger, C. M., Mühle, J., Henne, S., Rigby, M., et al. (2017). Atmospheric histories and emissions of chlorofluorocarbons CFC-13 ($CClF_3$), σCFC-114 ($C_2Cl_2F_4$), and CFC-115, and CFC-115 (C_2ClF_5). *Atmospheric Chemistry and Physics*, *18*(2), 979–1002. https://doi.org/10.5194/acp-18-979-2018

Von Clarmann, T. (2013). Chlorine in the stratosphere. *Atmósfera*, *26*(3), 415–458. https://doi.org/10.1016/S0187-6236(13)71086-5

Waters, J., Froidevaux, L., Harwood, R., Jarnot, R., Pickett, H., Read, W., et al. (2006). The Earth observing system microwave limb sounder (EOS MLS) on the aura satellite. *IEEE Transactions on Geoscience and Remote Sensing*, *44*(5), 1075–1092. https://doi.org/10.1109/TGRS.2006.873771

Webster, C., May, R., Jaeglé, L., Hu, H., Sander, S., Gunson, M., et al. (1994). Hydrochloric acid and the chlorine budget of the lower stratosphere. *Geophysical Research Letters*, *21*(23), 2575–2578. https://doi.org/10.1029/94GL02806

Western, L. M., Rigby, M., Mühle, J., Krummel, P. B., Lunder, C. R., O'Doherty, S., & Prinn, R. G. (2025a). Global emissions and abundances of chemically and radiatively important trace gases from the AGAGE network [Dataset]. *Zenodo*. https://doi.org/10.5281/zenodo.15586140

Western, L. M., Daniel, J. S., Vollmer, M. K., Clingan, S., Crotwell, M., Fraser, P. J., et al. (2024). A decrease in radiative forcing and equivalent effective chlorine from hydrochlorofluorocarbons. *Nature Climate Change*, *14*(8), 805–807. https://doi.org/10.1038/s41558-024-02038-7

Western, L. M., Rigby, M., Mühle, J., Krummel, P. B., Lunder, C. R., O'Doherty, S., et al. (2025b). Global emissions and abundances of chemically and radiatively important trace gases from the AGAGE network. *Earth System Science Data Discussions*, *17*(1), 6557–6582. https://doi.org/10.5194/essd-17-6557-2025

WMO. (2018). WMO (World Meteorological Organization), scientific assessment of ozone depletion: 2018 (Technical Report) (p. 588). Global Ozone Research and Monitoring Project - Report No. 58.

WMO. (2022). *World Meteorological Organization (WMO), scientific assessment of ozone depletion: 2022 (Technical Report)*. GAW Report No. 278 (p. 509). WMO.

Zander, R., Gunson, M. R., Farmer, C. B., Rinsland, C. P., Irion, F., & Mahieu, E. (1992). The 1985 chlorine and fluorine inventories in the stratosphere based on ATMOS observations at 30° north latitude. *Journal of Atmospheric Chemistry*, *15*(2), 171–186. https://doi.org/10.1007/BF00053758

Erratum

The originally published version of this article contained a formatting error in the main text and the caption to Figure 8. Specifically, altitude range indicators in the notation of modified total chlorine profiles were incorrectly formatted as bracketed suffixes rather than superscripts. The corrections are as follows: Cltot[0–15] has been corrected to $Cl_{tot}^{0–15}$, Cltot[0–61] has been corrected to $Cl_{tot}^{0–61}$, and Cltot[20–61] has been corrected to $Cl_{tot}^{20–61}$. This formatting error occurred in nine instances within Section 4.4: in the sixth and eighth sentences of the third paragraph, in the second, fourth, and sixth sentences of the fourth paragraph; and in the ninth sentence of the fifth paragraph. Four instances were corrected in the caption for Figure 8. These have been corrected to the proper superscript format. This may be considered the authoritative version of record.